

Topical Editor Decision: Publish subject to minor revisions (review by editor) (05 Oct 2020) by [Joachim Gottsmann](#)

Comments to the Author:

Dear Authors,

I have had a look at your revised ms. I am sorry to report that the language issue is far from being resolved. To give an example, the first few sentences of the abstract are full of syntax and grammatical errors and hard to follow. I hence have to assume that you have not taken my earlier recommendation seriously.

I am giving you one more chance to revise the ms according to my earlier recommendations regarding the use of English. You should consider having the ms proof read by a native speaker or professional editing services.


Should I find the next (third) revision not according to the Journal's publication standards, I will not hesitate to reject the paper altogether.

With best wishes,
Jo Gottsmann
Executive Editor SE

Dear Editor,

we are sorry about your last comment. We tried to improve the manuscript as much as possible and we thought was OK, but unfortunately it wasn't. Following your suggestion, the manuscript was sent to a proof read professional editing service (see the attached email). We hope that this revised version is fine. Please note that in the current version the references list is not still formatted because we plan to submit a LaTeX version, if the paper will be accepted for the publication.

We look forward to hearing from you,
Best regards,
Silvia Massaro

From: Lucia Capra Pedol lcapra@geociencias.unam.mx 
Subject: Fwd: Proofreading complete: Analysing stress field conditions of the Colima Volcanic Complex (ref. no. 202010-5172859)
Date: 9 October 2020 at 13:56
To: Silvia Massaro silvia.massaro@ingv.it, robertosulpizio Roberto roberto.sulpizio@uniba.it

LP

va

ciao
Lucia

----- Forwarded message -----

De: PRS <accoedj@gmail.com>
Date: vie., 9 de oct. de 2020 a la(s) 05:51
Subject: Proofreading complete: Analysing stress field conditions of the Colima Volcanic Complex (ref. no. 202010-5172859)
To: <lcapra@geociencias.unam.mx>

Proof-Reading-Service.com
PhD theses, journal papers, books and other professional documents

Proof-Reading-Service.com Ltd, Devonshire
Business Centre, Works Road, Letchworth Garden
City, Hertfordshire, SG6 1GJ, United Kingdom
Office phone: +44(0)20 31 500 431
E-mail: enquiries@proof-reading-service.com
Internet: <http://www.proof-reading-service.com>
VAT registration number: 911 4788 21
Company registration number: 8391405

Dear Lucia Capra,

We have completed the proofreading you asked for. Please find attached two versions of each document. One is the tracked version, showing all the changes our proofreader has made. You can use the tracking function of Word to accept or reject each change individually. The second is the clean version, which you can use if you do not wish to review the changes we have made. Please note there may be some comments from the proofreader in both versions.

If the clean version still shows corrections please follow the following steps: Press Ctrl+Shift+E and you should see in the task bar a new menu, click on the drop down menu and select 'Final'.

When you are submitting or resubmitting your article to a scientific or academic journal, remember to inform the journal editor in your covering letter that your paper has been professionally proofread. We will be delighted to provide you with verification that your article has been proofread by PRS, so please request a certificate to accompany your paper, especially if the journal editor has already indicated a need for professional proofreading.

If you have further questions about the proofreading, feel free to get in touch.

Thank you for using our service this time. We would be very happy to provide you with further services in the future!

We have recently been experiencing some problems with emails and attachments from some University and business accounts. If you have not heard from us within 2 hours during normal business hours after you have sent your work it is possible that your email has not been received. Please send it from a webmail account such as Hotmail, Yahoo or GMAIL.

Yours sincerely

Emma Taylor





Analysing stress
field co...n.docx



Analysing stress
field co...n.docx

Analysing stress field conditions of the Colima Volcanic Complex (Mexico) by integrating FEM simulations and geological data

Silvia Massaro^{1,2}, Roberto Sulpizio^{1,2,3}, Gianluca Norini², Gianluca Groppelli², Antonio Costa¹, Lucia Capra⁴, Giacomo Lo Zupone⁵, Michele Porfido⁶, Andrea Gabrieli⁷

¹Istituto Nazionale di Geofisica e Vulcanologia, Via D. Creti 12, 40128, Bologna, Italy

²Istituto di Geologia Ambientale e Geoingegneria, Consiglio Nazionale delle Ricerche, Via M. Bianco 9, 20131, Milan, Italy

³Dipartimento di Scienze della Terra e Geoambientali, Via E. Orabona 4, 70125, Bari, Italy

⁴Centro de Geociencias, Universidad Nacional Autonoma de Mexico, Queretaro, Mexico

⁵Institute of New Energy and Low-carbon Technology, Sichuan University, Chengdu, PRC

⁶Alumni Mathematica, Dipartimento di Matematica, Via E. Orabona 4, 70125, Bari, Italy

⁷Hawai'i Institute of Geophysics and Planetology, 1680 E-W Road, Honolulu, Hawai'i 96922, USA

*Corresponding author: Silvia Massaro (silvia.massaro@ingv.it).

Abstract

In recent decades, Finite Element Modelling (FEM) has become a very popular tool in volcanological studies, and has been used to describe even complex system geometries, accounting for multiple reservoirs, topography and heterogeneous distribution of host rock mechanical properties. In spite of this, the influence of geological information on numerical simulations is still poorly considered. In this work, a 2D Finite Element Modelling FEM of the Colima Volcanic Complex (Mexico) is provided by using the Linear Static Analysis (LISA) software, in order to investigate the stress field conditions at increasing detail of geological data. By integrating the published geophysical, volcanological and petrological data, we modelled the stress field considering either one or two magma chambers connected to the surface via dykes or isolated (not connected) in the elastic host rocks (considered homogeneous and non homogeneous). We also introduced tectonic disturbance, considering the effects of direct faults bordering the Colima Rift and imposing an extensional far-field stress of 5 MPa. We ran the model using gravity in the calculations. Our results suggest that an appropriate set of geological data is of pivotal importance for obtaining reliable numerical outputs, which can be considered as a proxy for natural systems. Beside and beyond the importance of geological data in FEM simulations, the model runs using the complex feeding system geometry and tectonics show how the present-day Colima volcanic system can be considered in equilibrium from any stress state point of view, in agreement with the long-lasting open conduit dynamics that have lasted since 1913.

ha eliminato: .

ha eliminato: .

ha eliminato: .

ha eliminato: .

ha eliminato: .

ha eliminato: .

ha eliminato: .

ha eliminato:

ha eliminato: .

ha eliminato:

Formattato: Controlla righe isolate

47 **1 Introduction,**

48

49 Magmatism and tectonism are strongly related to regional and local stress fields, affecting both the
50 orientation of faults and the location of volcanic vents (Geyer et al., 2016). The stress field around a
51 magmatic source originates from three main contributions: (1) the background stress, composed of a
52 vertical gravitational load, a lateral horizontal load (lithostatic confinement), and tectonic regime;
53 (2) the stress field caused by the loading of the volcano edifice; and, (3) the stress field generated by
54 the magmatic pressure (e.g. Martí and Geyer, 2009; Currenti and Williams et al., 2014). In recent years,
55 a large number of semi-analytical and numerical methods have been proposed for the solution of the
56 stress field state of natural systems (e.g. Cayol and Cornet, 1998; Simms and Garven, 2004; Manconi
57 et al., 2007; Long and Grosfils, 2009; Currenti et al., 2010; Currenti and Williams et al., 2014; Zehner
58 et al., 2015), taking into account the static elastic deformation in a multi-layered half-space (e.g.
59 Dieterich and Decker, 1975; Bonafede et al., 2002; Wang et al., 2003; Gudmundsson and Brenner,
60 2004; Pritchard and Simons, 2004; Zhao et al., 2004; Pritchard and Simons, 2004; Gottsmann et al.,
61 2006; Geyer and Gottsmann, 2010; Zhong et al., 2019). Following the successful application in
62 mechanical engineering, fluid dynamics and thermodynamics (e.g., Gutiérrez and Parada, 2010;
63 Gelman et al., 2013), the use of Finite Element Modelling method (FEM) has been introduced extensively
64 introduced in volcanology, in order to investigate the effects of topography, lithologic heterogeneities,
65 tectonic stresses and the gravity field on the stress state of volcanic systems (e.g. Fujita et al., 2013;
66 Bunney, 2014; Carcho and Galán del Sastre, 2014; Hickey et al., 2015; Bunney, 2014; Ronchin et al.,
67 2015; Hickey et al., 2015; Cabaniss et al., 2019; Rivalta et al., 2019).

68 There are several examples of the use of FEM for volcanic systems, which has several examples, which
69 spanning from the influence of layered materials on the surface deformation process during volcanic
70 inflation (e.g. Darwin volcano, Galapagos Islands; Manconi et al., 2007; Albino et al., 2010) to
71 processes affecting chamber rupture (e.g. Grosfils, 2007; Long and Grosfils, 2009).

ha eliminato:

Formattato: Controlla righe isolate

ha eliminato: the

ha eliminato: ,

ha eliminato:)

ha eliminato:

ha eliminato:

78 The local stress around a volcanic feeding system depends on the geometry of the magma plumbing
79 system, including [the](#) chamber(s) and dykes forming it, and on the mechanical properties of the host
80 rock around it (e.g. [Martí and Geyer, 2009](#)), and especially on changes in Young modulus (e.g.
81 Gudmundsson et al., 2011; [Jeanne et al., 2017](#); [Heap et al., 2020](#)). For instance, limestone, lava flows,
82 welded pyroclastic deposits and subvolcanic rocks can be very stiff (high Young modulus; ca. 1.7–
83 27 GPa for limestones, [Touloukian, 1981](#); ca. 5.4 GPa for volcanic rocks, [Heap et al., 2020](#)), but young
84 and non-welded pyroclastic units may be very soft (low Young modulus; ca. 1.7–3.1 GPa, [Margottini](#)
85 [et al., 2013](#)). Therefore, the local stress may change abruptly change from one layer to another (e.g.,
86 [Gudmundsson, 2006](#)). Irrespective of the scope of the numerical investigation, the importance of
87 applying accurate physical constraints to FEM [h](#)was already been discussed in many studies (e.g., [Folch](#)
88 [et al., 2000](#); [Fernandez et al., 2001](#); [Newman et al., 2001](#); [Fernandez et al., 2001](#); [Currenti et al., 2010](#);
89 [Geshi et al., 2012](#)). However, in the last decade, few investigations have been carried out to assess the
90 influence of the amount and quality of geological data ointo FEM computations ([Kinvig et al., 2009](#);
91 [Norini et al., 2010, 2019](#); [Cianetti et al., 2012](#); [Ronchin et al., 2013](#); [Chaput et al., 2014](#); [Norini et al.,](#)
92 [2019](#)). To bridge this gap, in this work we used the LInear Static Analysis (LISA) software (version
93 8.0; [www.lisafea.com](#)) to study the subsurface stress field state inat the Colima Volcanic Complex
94 (CVC, Mexico) at increasing geological detail.

95 The CVC area is a good candidate for testing the response of FEM software against different geological
96 conditions, being constituted by a large volcanic complex ([Lungarini et al., 2005](#)) within a tectonic
97 graben filled with volcanoclastic material ([Fig. 1a](#); [Norini et al., 2010, 2019](#)). The FEM was run starting
98 from simple homogeneous [vs](#) stratified lithology of [the](#) subsurface, and [in](#) successively [more](#) detail by
99 the addition of single and double magma chambers, feeder dykes, faults, and extensional far-field
100 tectonic stress ([Fig. 1b](#)).

ha eliminato: i

ha eliminato: s

ha eliminato: -

ha eliminato:

ha eliminato: modelling

ha eliminato: .

ha eliminato: ed

ha eliminato: ,

ha eliminato:

101

102

112 **2 The Colima Volcanic Complex (Mexico)**

113

114 *2.1 Geological framework*

115 The Pleistocene–Holocene CVC is one of the most prominent volcanic edifices within the Trans-
116 Mexican Volcanic Belt (TMVB) (Macías et al., 2006; Capra et al., 2016; Norini et al., 2019; Fig. 1a).
117 In this area, the Rivera microplate and the Cocos plate subduct beneath the North America plate along
118 the Middle American Trench (Stock and Lee, 1994), forming a triple junction that delimits the tectonic
119 units known as the Jalisco Block (JB) and the Michoacán Block (MB) (Luhr et al., 1985; Allan, 1986;
120 Rosas-Elguera et al., 1996, 1997; Ferrari and Rosas-Elguera, 1999; Rosas-Elguera et al., 2003; Frey et
121 al., 2007). The three rifts of this system are the Tepic–Zacoalco Rift (TZR), Chapala–Tula Rift (CTR),
122 and Colima Rift (CR). The still-active NS-trending CR was formed during a rifting phase which
123 occurred after the Late Cretaceous–Paleogene compressive and transpressive phase (Allan, 1986; Serpa
124 et al., 1992; Bandy et al., 1995; Cortés et al., 2010). While opening, the CR was gradually filled with
125 Pliocene–Quaternary lacustrine sediments, alluvium and colluvium (e.g. Allan, 1986; Allan et al.,
126 1991; Norini et al., 2010). The geometry, kinematics and dynamics of the CR have been studied on the
127 basis of field, seismic and geodetic data, mainly collected in its northern and central sectors (see Fig. 1
128 in Norini et al., 2010).

129 The magnitude of vertical displacement of the northern and central sectors is ca. 2.5 km by adding the
130 topographic relief of the bounding fault scarps (1.5–1.6 km) to the calculated sediment depth (Allan,
131 1985; Serpa et al., 1992). Field data and focal mechanism solutions are consistent with a direction of
132 opening of the northern and central sectors oriented from E–W to NW–SE, with mainly normal and
133 minor right-lateral displacements of the bounding faults (Barrier et al., 1990; Suárez et al., 1994; Rosas-
134 Elguera et al., 1996; Garduño-Monroy et al., 1998; Norini et al., 2010, 2019). In contrast to field and
135 seismic evidence of long-term slightly dextral oblique extension, recent GPS geodetic measurements
136 suggest a possible left oblique extension of the CR (Selvans et al., 2011). In both cases, the stress

Formattato: Mantieni con il successivo

ha eliminato: -

Formattato: Controlla righe isolate

ha eliminato: ,

ha eliminato: ; Rosas-Elguera et al.

ha eliminato: :

ha eliminato: -

ha eliminato: the

ha eliminato: -

ha eliminato: ,

ha eliminato: the

ha eliminato: :

ha eliminato: -

ha eliminato: :

ha eliminato: ,

ha eliminato: .

ha eliminato: -

ha eliminato: -

ha eliminato: a

153 regime is extensional with an E-W orientation of the minimum horizontal stress in the CVC basement
 154 (Barrier et al., 1990; Suárez et al., 1994; Rosas-Elguera et al., 1996; [Norini et al., 2010](#); Selvans et al.,
 155 2011; Norini et al., 2019).
 156 The CVC stands within the central sector of the CR, on top of Cretaceous limestone, Late Miocene–
 157 Pleistocene volcanic rocks, and Pliocene–Holocene lacustrine sediments, alluvium and colluvium
 158 (Allan, 1985, 1986, 1991; Cortés, 2005; Norini et al., 2010; Escudero and Bandy, 2017). It is formed
 159 by three andesitic stratovolcanoes: Cantaro (2900 m a.s.l.), Nevado de Colima (4255 m a.s.l.) and, in
 160 the southern part, the youngest and active Volcàn de Colima (3763 m a.s.l.) (Norini et al., 2019 and
 161 reference therein; Fig. 1a).

- ha eliminato: -
- ha eliminato: 2010,
- ha eliminato:
- ha eliminato: the
- ha eliminato: s
- ha eliminato: -
- ha eliminato: ,
- ha eliminato: -
- ha eliminato: ,
- ha eliminato: ès

163 *2.2 Eruptive activity*

164 The eruptive history of the CVC started in the northeast area with the formation of Cantaro volcano at
 165 ca. 1–1.5 Ma followed by Nevado de Colima at ca. 0.53 Ma, which is composed of voluminous
 166 andesitic lava domes and deposits associated with caldera-forming eruptions and partial sector
 167 collapses (Robin et al., 1987; Roverato et al., 2011; Roverato and Capra, 2013; Cortés et al., 2019).
 168 The youngest – Volcàn de Colima – comprises the Paleofuego edifice, which suffered several sector
 169 collapses that formed a horseshoe-shaped depression where the new active cone (also known as Volcàn
 170 de Fuego) grew up. Its activity was characterized by dome growths and collapses, extrusion of lava
 171 flows, and Vulcanian and occasionally sub-Plinian explosive eruptions (Saucedo et al., 2010; Massaro
 172 et al., 2018, 2019).

- Formattato: SpazioDopo: 10 pt, Controlla righe isolate
- ha eliminato:
- Formattato: SpazioDopo: 0 pt, Controlla righe isolate
- ha eliminato: -
- ha eliminato:
- ha eliminato: ès
- ha eliminato:
- ha eliminato: cone
- ha eliminato: s
- ha eliminato:

174 *2.3 The CVC plumbing system*

175 Seismic tomography (Spica et al., 2017) highlights a 15 km-deep low velocity body (LVB), which was
 176 interpreted as a deep magma reservoir. It is confined within the CR, suggesting a structural control of
 177 the normal fault system on it (Spica et al., 2014). The LVB has an extent of ca. 55 km × ×30 km in

- Formattato: SpazioDopo: 10 pt, Controlla righe isolate
- Formattato: SpazioDopo: 0 pt, Controlla righe isolate
- ha eliminato: the

197 the N–S and E–W directions, respectively, showing an averaged thickness < 8 km. Escudero and
198 Bandy (2017) obtained a higher- resolution tomographic image of the CVC subsurface area, showing
199 that the most active magma generation zone is now under the Fuego de Colima edifice. The ambient
200 seismic noise tomographic study of Spica et al. (2014) indicates a shallow magma chamber above ca.
201 7 km depth, in agreement with petrological studies (Medina-Martinez et al., 1996; Luhr, 2002; Zobin
202 et al., 2002; López-Loera et al., 2011; Reubi et al., 2013, 2019; Macíasias et al., 2017; Reubi et al.,
203 2019). Cabrera-Gutiérrez and Espíndola (2010) suggested the shallow active magma storage has a
204 volume of ca. . 30 30 km³. It is connected to the surface by conduits, whose path is facilitated by the
205 presence of the CR fault zone, which provide a natural pathway for fluids (e.g., Allan, 1986; Norini et
206 al., 2010, 2019). The arrangement of dykes and the alignment of the volcanic centres of the CVC
207 suggest that the dykes swarms draining the magma chambers developed along the NNE–SSW-
208 trending, steep, eastward- dipping normal fault exposed on the northern CVC flank (Norini et al., 2010,
209 2019).

210 Massaro et al. (2018) provided a first-order geometrical reconstruction of the Fuego de Colima feeding
211 system during the 1913 sub-Plinian eruption, using volcanological data (Saucedo et al., 2010; Bonasia
212 et al., 2011; Saucedo et al., 2011) as inputs and constraints for numerical simulations. Results showed
213 good matches for a hybrid configuration of the shallow conduit feeding system composed of a ca, 5500
214 5500 m- long, 200–2000 m- wide, and 40 m width dyke passing into a shallower (500 m long, 40 m
215 diameter) cylindrical conduit. The shallow magma chamber top was set at 6 km of depth, and dyke–
216 cylinder transition at 500 m below the summit as inferred from geophysical data (Salzer et al., 2014;
217 Arámula et al., 2018).

218

219

ha eliminato: by

ha eliminato: , 2011

ha eliminato: -

ha eliminato: .

224 **3 Methods**

225

226 In this study, we used the commercial 8.0 version of LISA (www.lisafea.com), a general-purpose Finite
227 Element Analysis (FEA) software [program](#) developed in the 1990s and based on the formulations
228 proposed by Rao (1989), and successively integrated from other sources (Bathe, 1990; Michaeli, 1991;
229 Schwarz, 1991; Babuska et al., 1995). Despite LISA originally [being](#) used for structural analysis (Rao,
230 1989, 2013), it successfully predicts the stress-strain behaviour of rock masses in elastic models, in
231 particular the deformation mechanisms even in layered rock masses (Gabrieli et al., 2015).

232

233 *3.1 Modelling approach*

234 The stress field of the CVC plumbing system is simulated considering an E-W cross-section, parallel
235 to the extension associated with the active CR (Norini et al., 2010, 2019) as shown in Figure 1a-b (a-
236 a').

237 Since the extent of the CVC magma chambers in the NNE-SSW direction is typically much longer
238 than the dimensions of the E-W cross-section (Spica et al., 2017), 2D solutions of either numerical or
239 analytical models describing E-W elongated magma chambers in the crust can be reasonably adopted
240 (Jaeger et al., 2009; Costa et al., 2011). A topographic profile and 2D plane along the chosen E-W
241 cross-section of the CVC area was obtained in ESRI ArcGIS from a Digital Elevation Model (DEM,

242 resolution 50 m; Instituto Nacional de Estadística y Geografía → INEGI <https://en.www.inegi.org.mx/>)
243 and imported into Autodesk Auto-Cad R13 using a third-degree spline approximation. The IGES file
244 was then imported into LISA for the mesh discretization.

245 The investigated domain extends 60 × 30 km in an x-z Cartesian Coordinate System with three- and
246 four-node finite element discretization (Table 1). Zero normal displacements are assigned at the bottom
247 and the lateral boundaries, while the upper boundary represents the free-stress ground surface (Fig. 1c).

Formattato: Mantieni con il successivo

Formattato: SpazioDopo: 0 pt, Controlla righe isolate

ha eliminato: '

ha eliminato: was

ha eliminato: ;

ha eliminato: -

ha eliminato:

Formattato: SpazioDopo: 10 pt, Controlla righe isolate

Formattato: Controlla righe isolate

ha eliminato: -

ha eliminato: o

ha eliminato: ;

ha eliminato: -

ha eliminato: -

ha eliminato: -

ha eliminato: -

ha eliminato:

ha eliminato: -

ha eliminato: -

ha eliminato: (

ha eliminato: -

ha eliminato:

ha eliminato: x

ha eliminato: -

ha eliminato: a

269 The FEM is carried out using a plane strain approximation, implying that the deformation in the third
270 direction is assumed to be negligible.

ha eliminato: by

ha eliminato:

271 As reported by Zehner et al. (2015), FEM of geological structures requires accurate discretization of

ha eliminato: in

Formattato: SpazioDopo: 0 pt, Controlla righe isolate

272 the computational domain. It follows that the unstructured tetrahedral meshes have to fulfil the
273 following requirements: i) sufficient mesh quality: the tetrahedrons should not be too acute-angled,

ha eliminato: s

274 since numerical instabilities can occur; ii) incorporation of geometry for defining boundary conditions

ha eliminato: .

275 and constraints; and iii) local adaption, which is a refinement of the mesh in the vicinity of physical

ha eliminato: .

276 sources in order to avoid numerical errors during the simulation. In this work, we adopted a mesh
277 composed of 4660 plane continuum elements, which have been refined in the regions of higher
278 gradients (i.e. near the contours of the magmatic feeding system).

279 In our simulations, the extent of the rock layers (Table 2) refers to that used by Norini et al. (2010,
280 2019). The configuration of the CVC feeding system (i.e. depth, shape and dimensions of the magma

Formattato: Controlla righe isolate

ha eliminato: is

ha eliminato: red

281 chambers and feeder dykes) derives from the literature (Spica et al., 2014, 2017; Massaro et al., 2018,

282 2019) and is simplified in Figure 1d. In particular, magma chambers and dykes are considered as

ha eliminato: it

283 pressurized finite-size bodies in an elastic crustal segment, acting as fluid-filled holes. The boundary
284 condition (pressurization) is provided by applying internal forces that act on the walls. This approach

285 has been used extensively in several analytical and numerical models that treat magma reservoirs as

ha eliminato: used

286 internally pressurized ellipsoidal cavities within an elastic half-space, in order to gain insight into the
287 behaviour of magma plumbing systems (Pinel and Jaupart, 2004; Gudmundsson, 2006; Grosfils, 2007;

ha eliminato:

288 Andrew and Gudmundsson, 2008; Hautmann et al., 2013; Currenti and Williams, 2014; Zhong et al.,

289 2019).

ha eliminato:

290 Previously published studies indicate that differences between, and problems with, elastic models

291 derive principally from the key role played by gravity (e.g. Lister and Kerr, 1991; Watanabe et al.,

292 2002; Gerbault, 2012; Albino et al., 2018; Gerbault, 2012; Lister and Kerr, 1991; Watanabe et al., 2002).

ha eliminato: ;

293 Some authors have argued ondiscussed whether or not it is appropriate or not to account for the gravity

294 body force in models of volcanic systems (e.g. Currenti and Williams, 2014; Grosfils et al., 2015).

308 When the gravitational loading is not included in the model, the volcanic deformation results from a
309 change with respect to a stage previously at equilibrium (e.g. Gerbault et al., 2018). In this work, we
310 carried out simulations considering the effect of the gravitational loading in the host rock, implemented
311 via body forces. The model initial condition has a pre-assigned lithostatic stress, whose computation,
312 in the presence of topographical and material heterogeneities, is not trivial because it requires
313 application of the gravity load, preserving the original non-deformed geometry of the mesh
314 (Cianetti et al., 2012). Since due to the presence of a lithostatic stress field, the load applied at the
315 reservoir boundaries represents a superposition of the magmatic pressure and lithostatic component.
316 We define here the magmatic pressure as either excess pressure (ΔP_e , magmatic minus lithostatic
317 pressure but below the tensile strength of wall rocks) or over pressure (or driving pressure ΔP_o , which
318 is the magmatic pressure exceeding the tensile strength of wall rocks; Gudmundsson, 2012). The first
319 pertains to the FEMs using isolated magma chambers (single or double), while the second is used for
320 models with connected magma chambers (with conduit/feeding system).

321 We also took into account the effect of the existing faults of the CR system even though LISA cannot
322 include a frictional law to represent the fault movement (i.e. Chaput et al., 2014). As reported by
323 Jeanne et al. (2017 and reference therein), the damage induced by faults increases from the host rocks
324 to the fault core, implying the a reduction in the effective elastic moduli. In this light, we represented
325 the faults bordering the CR as two damage zones (ca. 70° of inclination, ca. 1 km thick, and down to
326 10 km of depth) showing reduced elastic properties with respect to the surrounding host rocks.

327 To take into account the effect of the far-field extensional regime, we applied a uniform stress of 5
328 MPa to the lateral boundaries of the domain (as reported by Marti and Geyer, 2009).
329 Considering the E-W cross-section (a-a'; Fig. 1a), we provided six domain configurations: i) a
330 “homogeneous lithology model” in which the volcanic domain is only composed of andesite rocks;
331 ii) a “non-homogeneous lithology model” where different geological units are considered; iii) a
332 “single magma chamber model” composed of a not homogeneous lithology and a 15 km-deep magma
333 chamber with non-homogeneous lithology; iv) a “dual magma chamber model” composed of a non-

ha eliminato: if

Formattato: SpazioDopo: 0 pt, Controlla righe isolate

ha eliminato:

ha eliminato: in

ha eliminato: i

ha eliminato:

ha eliminato: -

ha eliminato: -

Formattato: Nessuna, SpazioDopo: 0 pt

341 -homogeneous and 6 km- and 15 km-deep magma chambers; v) a “conduit feeding system model”
342 composed of non-t homogeneous lithology, 6 km- and 15 km-deep magma chambers connected
343 through a deep dyke evolving into a shallow conduit near the surface; vi)) an “extensional model”,
344 with a 5 MPa horizontal extensional stress (far field); and, vii) a “faulted model”, in which are also
345 added two damaged zones mimicking the CR faults (local stress) are also added (Fig. 1b).

346 The number of nodes is set at 4426 for the only substratum and single magma chamber models, at 4161
347 for the dual magma chamber model, and at 3737 for the conduit feeding system and faulted models,
348 It is important to note that simulation outputs are shown using different colour scales. Although such a
349 choice may make difficult visual comparison of the different runs difficult, it preserves the necessary
350 details of stress distribution, which would have been lost using a common colour scale.

351 Finally, in the following we refer to σ_1 as the greatest compressive stress and σ_3 as the least compressive
352 stress.

353
354

355 4 Geological data

356

357 4.1 Stratigraphy and rock mechanics

358 Four units forming the CVC system are defined from the available geological data (Table 2):
359 i) basement (Unit B): Cretaceous limestones and intrusive rocks forming the bed-rock underlying the
360 CVC; ii) graben fill deposits (Unit GF): Quaternary alluvial, colluvial, and lacustrine deposits filling
361 the graben; iii) Fuego de Colima deposits (Unit FC): andesitic lavas and pyroclastic deposits forming
362 the Paleofuego—Fuego de Colima edifices; and iv) Volcaniclastic deposits (Unit VD): volcaniclastic
363 deposits covering the southern flank of the CVC (e.g. Cortés et al., 2010; Norini et al., 2010, 2019).

364 We assumed constant mechanical characteristics within each unit using the typical rock mass properties
365 of density (ρ), Young modulus (E) and Poisson ratio (ν) (Table 2). The rock masses are considered dry,

ha eliminato: in

ha eliminato: is set at 4426

ha eliminato: is set at 4161,

ha eliminato:

Formattato: Controlla righe isolate

ha eliminato:

ha eliminato: s

ha eliminato: result into a

Formattato: SpazioDopo: 0 pt, Controlla righe isolate

ha eliminato: i

Formattato: SpazioDopo: 10 pt, Controlla righe isolate

Formattato: SpazioDopo: 10 pt, Controlla righe isolate

Formattato: SpazioDopo: 0 pt, Controlla righe isolate

ha eliminato:)

Formattato: Controlla righe isolate

ha eliminato: ,

376 in order for (eventual) pore pressure to be neglected. Only for Unit GF was a higher value for the
 377 Poisson ratio used close to the surface in order to mimic the high water content in the graben sediments.
 378 The maximum thickness of the graben fill (about 1 km) is assumed from the literature (Allan, 1985;
 379 Serpa et al., 1992; Norini et al., 2010, 2019). For Units B and GF, rock mass proprieties are derived
 380 from Hoek and Brown (1997) and Marinos and Hoek (2000), while for volcanic materials (units FC
 381 and VD; Table 2) they are estimated according to the approach proposed by Del Potro and Hürlimann
 382 (2008). In order to describe the effects of the CR faults on stress field distribution, the mechanical
 383 properties are locally degraded in proximity to the faults themselves.

ha eliminato: was

385 4.2 *Geometry of the plumbing system*

386 In our 2D model, we assume the CVC is composed of two magma chambers connected by dykes and
 387 to the surface by a conduit (Fig. 1d). The shape of the magma chambers and dykes is represented by
 388 elliptical cross-sections with the major axis ($2a$) and minor axis ($2b$) axes.

ha eliminato: The

Formattato: SpazioDopo: 10 pt, Controlla righe isolate

Formattato: Controlla righe isolate

ha eliminato: a

ha eliminato: are

389 Generally, magma chambers have a sill-like shape that is often imaged in seismic studies of volcanoes
 390 and rift zones (Macdonald, 1982; Sinton and Detrick, 1992; Mutter et al., 1995; MacLeod and
 391 Yaouancq, 2000; Singh et al., 2006; Canales et al., 2009). Most of them are not totally molten but rather
 392 a mixture of melt and crystal mush (i.e. Parfitt and Wilson, 2008). Various estimates have been made
 393 to infer the actual amount of melt in a magmatic body, showing that it is only ca. 10% of the total
 394 chamber volume (Gudmundsson et al., 2012 and reference therein).

ha eliminato: the

395 After Spica et al. (2017), the 15 km-deep LVB is ca. 7000 km³; therefore, if we assume the melt as
 396 10% melt, the deep magma chamber volume would be ca. 700 km³. Simplifying this volume in an
 397 elliptical sill-like geometry, the magma chamber dimensions (i.e. $2a$, $2b$ and $2c$ axes) have to be scaled
 398 according to the LVB (55 x 30 x 8 km; Spica et al., 2017) using $2a = 14$ km, $2b = 3.6$ km and $2c = 26$
 399 km, $2c$ being elongated in an NW-SE direction. For the shallow part of the feeder system, we have no
 400 detailed geophysical constraints. However, Massaro et al. (2019) reproduced through numerical

ha eliminato:

ha formattato: Tipo di carattere: 12 pt

ha eliminato: -

ha formattato: Tipo di carattere: Non Corsivo

ha eliminato: ,

ha eliminato:

ha eliminato: ×

ha eliminato: ×

ha eliminato: ,

ha eliminato: being

ha eliminato: -

416 modelling the nonlinear cyclic eruptive activity at Fuego de Colima in the last 20 years, using a shallow
 417 magma chamber volume in the range of 20–50 km³, according to the estimation of Cabrera-Gutiérrez
 418 and Espíndola (2010). Here we assume a volume of 30 km³, using $2a = 3.5$ km, $2b = 2$ km and
 419 $2c = 8$ km as the dimensions of the shallow magma chamber.
 420 Numerous theoretical and field studies have established that host rock stresses dictate the magma
 421 pathways (e.g. Gudmundsson, 2011; Maccaferri et al., 2011, 2011). During ascent to the surface, the
 422 dykes align themselves with the most energy-efficient orientation, which is roughly perpendicular to
 423 the least compressive stress (e.g. Gonnermann and Taisne, 2015; Rivalta et al., 2019), providing the
 424 magma driving pressure remains small compared to the deviatoric stress (Pinel et al., 2017; Maccaferri
 425 et al., 2019). This behaviour, however, can be modulated in the presence of significant variations in
 426 the fracture toughness of the surrounding rock due to stratification (Maccaferri et al., 2010) or to old
 427 and inactive fracture systems (Norini et al., 2019).

428 Although for oblate magma chambers the propagation of dykes is most probable from the tip areas, in
 429 our simulations the orientation of dykes is assumed to be vertical, because of the preferential pathways
 430 represented by the CR fault planes (Spica et al., 2017).

431 We set the dimensions of the feeder dykes in agreement with Massaro et al. (2018): deep dyke $2ad =$
 432 2 km; shallow dyke $2a$ varies from 1 km at the bottom to 500 m in the upper part of the volcano; width
 433 of both deep and shallow dykes $2bd = 2b = 100$ m (Fig. 1d).

434 It is worth noting that it is outside the scope of this work to provide the conditions for rupture of the
 435 magma chamber, LISA accounting only for the elastic regime. For these reasons, we fixed ΔP_e and
 436 ΔP_o (for isolated and connected magma chamber models, respectively) in the range of 10–20 MPa
 437 for the 15 km-deep chamber, and 5 MPa for the 6 km-deep one. For the dykes and conduit, ΔP_o is set
 438 to 10 MPa in the deeper dyke and 5 MPa in the shallower one, while in the upper 500 m of conduit it
 439 is 0.4 MPa.

ha eliminato: -

ha eliminato: ,

ha formattato: Tipo di carattere: Non Corsivo

ha formattato: Tipo di carattere: Non Corsivo

ha eliminato:

ha eliminato: ; Gudmundsson

ha eliminato:

ha formattato: Tipo di carattere: 10 pt

ha eliminato: 2

ha eliminato:

ha eliminato: ing

ha eliminato: rupture

ha eliminato: being

ha eliminato:

451 **Results**

452

453 In this section, we report the sensitivity analysis carried out to quantify approximation of the Young
454 modulus variation on FEM outputs, and description of the model outputs when adding complexity to
455 the input geological/geophysical data.

456

457 *5.1 Sensitivity analysis of Young modulus*

458 Using the single magma chamber model as a reference case, we quantified the influence of Young
459 modulus variation in each geological unit. Taking into account the mechanical properties of rocks
460 (Table 2) as reference values, we compared the stress state of the computational domain on changing
461 Young modulus by (\pm) one order of magnitude. This sensitivity analysis, although incomplete, may
462 lead to raised awareness on the selection of input data when running an FEM. The sensitivity analysis
463 was carried out on a reduced simulation domain (the x -axis was set to 35 km) in order to diminish the
464 influence of binding effects along the domain borders.

465 We applied the Euclidean norm (L2) method to illustrate the results. The L2 norm applied on a vector
466 space x (having components $i = 1, \dots, n$) is strongly related to the Euclidean distance from its origin,
467 and is equal to:

468

469
$$\|x\|^2 = \sqrt{\sum_i^n x_i^2} \quad (1)$$

470

471 In our case, the vector space x is composed of all nodes of the computational domain (Table 1). We
472 defined x_{ref} , the vector containing the results for the maximum and minimum principal stress, when
473 using the selected values of material properties (Table 1) and $x(-)$ and $x(+)$, the vectors on varying the
474 Young modulus by one order of magnitude in each unit.

Formattato: Mantieni con il successivo

ha eliminato:

ha eliminato: ed

ha eliminato: the

Formattato: Nessuna, SpazioDopo: 0 pt

ha eliminato: the

ha eliminato: the

ha eliminato: s

ha eliminato:

ha eliminato: at

ha eliminato:

ha eliminato: a

ha eliminato: f

ha eliminato: r

ha eliminato: ing

ha formattato: Tipo di carattere: Non Corsivo

ha formattato: Tipo di carattere: Non Corsivo

ha formattato: Tipo di carattere: Non Corsivo

ha eliminato: wi

ha eliminato: h

ha eliminato:

ha eliminato:

ha formattato: Tipo di carattere: 10 pt

ha formattato: Tipo di carattere: Non Corsivo

ha eliminato: -

ha formattato: Tipo di carattere: Non Corsivo

ha eliminato: ,

ha formattato: Tipo di carattere: Non Corsivo

ha eliminato: at

ha eliminato: of

496 In Figure 2 are reported the global relative variations in L2 of σ_1 and σ_3 caused by the variation of
 497 Young modulus in each unit, for each model configuration (i.e. non-homogeneous lithology, single
 498 magma chamber, dual magma chamber and dual magma chamber with conduits models) as follows:

$$\|x\|_{2(-)} = \|x_{ref} - x_{(-)}\|_2 / \|x_{ref}\|_2 \quad (2)$$

$$\|x\|_{2(+)} = \|x_{ref} - x_{(+)}\|_2 / \|x_{ref}\|_2 \quad (3)$$

503 All the models show variability of less than 15%, with a few exceptions within Unit B that have
 504 variability of over 30% (Fig. 2). In this light, the spatial distribution of the major variations seems not
 505 to significantly affect the final stress distributions, because: i) they are located near the mesh borders
 506 (Fig. 3a and b); and ii) when not at the mesh borders, the variations are limited to a few % (Fig. 3c
 507 and d). It means that a one order of magnitude variation in Young modulus produces variation in FEM
 508 outputs distributed over a large domain, and the change affecting the single nodes is limited to a few %.

510 5.2 Homogeneous and non-homogeneous lithology

511 In Figure 4 we report σ_1 and σ_3 stresses for gravity-loaded models with homogeneous lithology
 512 composed of only andesitic lavas (Fig. 4a) and non-homogeneous lithology composed of carbonates
 513 (Unit B) and alluvial, volcanoclastic and pyroclastic deposits (Units GF and VD; Fig. 4b). It is
 514 important to stress that the x_z zero displacement assigned at the bottom and at the lateral boundaries
 515 of the domain created substantial artefacts in the results (i.e. curved patterns of stress), especially
 516 considering σ_3 (Fig. 4, panels i and ii) where the boundary effect on the x -axis is amplified by the
 517 presence of the upper free surface. It follows that the only unperturbed area extends ca. 30 km
 518 horizontally and ca. 15 km vertically (within the blue contour in Fig. 4). It is worth noting that the
 519 homogeneous and non-homogeneous models show quite similar stress patterns results (Fig. 4).

ha eliminato:

ha eliminato: t

ha eliminato: ,

ha eliminato:

ha eliminato: not

ha eliminato: .

ha eliminato: .

ha eliminato: .

ha eliminato: .

ha eliminato: the

Formattato: SpazioDopo: 10 pt

ha eliminato: t

ha eliminato: ed

ha eliminato:

ha eliminato: by

ha eliminato: t

ha formattato: Tipo di carattere: Non Corsivo

ha eliminato: .

ha formattato: Tipo di carattere: Non Corsivo

ha eliminato: -

ha eliminato: -

ha eliminato: t

ha eliminato: results in

ha eliminato:

542 5.3 Gravitational modelling using inferred feeding system geometry

543 In Figures 5 and 6 we show three cross-section profiles describing the feeding system starting from a
544 single magma chamber to two chambers, then adding the conduits and, finally, considering the full
545 complexity by adding the effects of far-field stress and CR faults. Figure 5a describes σ_3 (panel i) and
546 σ_1 (panel ii) stress distribution for the single magma chamber model and $\Delta P_e = 10$ MPa. No significant

547 differences in the magnitude and pattern of stresses are visible using $\Delta P_e = 20$ MPa (Appendix 1a).

548 The addition of the shallow magma chamber significantly changes the values and pattern of both σ_3
549 and σ_1 (Fig. 5b). In particular, σ_3 and σ_1 stresses describe a typical inflation pattern produced by excess
550 pressure in the magma chamber(s) (Anderson, 1936; Gudmundsson, 2006, 2012), producing well-
551 defined stress arches of σ_3 (red dotted lines in Fig. 5bi) and divergent strong gradients of σ_1 around the
552 deep magma chamber (Fig. 5bii). Very slight differences in the magnitude and pattern of stresses
553 appear when using $\Delta P_o = 10$ MPa (Fig. 5b) or 20 MPa (Appendix 1b).

554 Looking at Figure 6, it is evident how insertion of the conduits in the CVC feeding system dramatically
555 changes the stress distribution, with the disappearance of the stress arch and a nearly constant stress in
556 the computational domain except around the deep magma chamber tips.

558 5.4 Application of an extensional stress field

559 In order to explore the influence of extensional far-field stress on stress patterns (Fig. 1a), we ran
560 simulations applying 5 MPa stress (typical low value for rift zones; Turcotte and Schubert, 2002;
561 Moeck et al., 2009; Maccaferri et al., 2014; Sulpizio and Massaro, 2017) along the lateral boundaries
562 of the computational domain (Fig. 7).

563 In the case of a single magma chamber ($\Delta P_e = 10$ MPa; Fig. 7, panels i and ii), the addition of the far-
564 field stress reduces the confinement effect due to the no displacement condition imposed along the x -
565 z directions (plane strain approximation). When considering the double magma chamber
566 configuration ($\Delta P_o = 10$ MPa in the deep chamber and $\Delta P_o = 5$ MPa in the shallower one), the presence

ha eliminato: the
Formattato: SpazioDopo: 10 pt

Formattato: Controlla righe isolate

ha eliminato: magma

ha eliminato: ,

ha formattato: Tipo di carattere: 12 pt, Non Apice / Pedice

ha formattato: Tipo di carattere: 10 pt

ha formattato: Tipo di carattere: 12 pt

ha formattato: Tipo di carattere: 12 pt, Non Apice / Pedice

ha formattato: Tipo di carattere: 12 pt

ha formattato: Tipo di carattere: 12 pt

ha formattato: Tipo di carattere: 12 pt, Non Apice / Pedice

ha formattato: Tipo di carattere: 12 pt, Non Apice / Pedice

ha formattato: Tipo di carattere: 12 pt

ha formattato: Tipo di carattere: 12 pt, Non Apice / Pedice

ha eliminato: ;

ha formattato: Tipo di carattere: 12 pt

ha eliminato: s

ha formattato: Tipo di carattere: 12 pt

ha formattato: Tipo di carattere: 12 pt, Non Apice / Pedice

ha eliminato:

Formattato: SpazioDopo: 0 pt, Controlla righe isolate

ha eliminato: the

ha eliminato:

Formattato: SpazioDopo: 10 pt

Formattato: Controlla righe isolate

ha eliminato: the

ha eliminato:

ha eliminato: u

ha eliminato:

ha eliminato: i

ha formattato: Tipo di carattere: Non Corsivo

580 of the far-field stress produces slight changes in stress magnitude and pattern for both σ_3 and σ_1 (Fig.
581 7, panels iii and iv) with respect to Figure 5b. Very similar effects appear in the complete feeding
582 system configuration model (Fig. 7, panels v and -vi). Also, in this case using $\Delta P_o = 20$ MPa in the
583 deep magma chamber does not significantly affect the model outputs (Appendix 2).

ha eliminato:
ha formattato: Tipo di carattere: 12 pt
ha formattato: Tipo di carattere: 12 pt
ha eliminato: -

585 5.5 Faults bordering the Colima Rift

586 The effect of faults bordering the CR on the final feeding system configuration is simulated through
587 two damage zones by degrading their elastic properties. Adding these elements does not significantly
588 alter the stress distribution observed in Figures 7v and 7vi, but only provides a slight reduction in both
589 σ_1 and σ_3 intensities around their edges (Figs. 7vii and 7viii). The different distance of the two damage
590 zones from the feeding system produces a small asymmetry in both σ_1 and σ_3 patterns with respect to
591 simulations without damage zones, especially near the deep magma chamber (Figs. 7v-viii).

Formattato: SpazioDopo: 10 pt
ha eliminato:
Formattato: Controlla righe isolate

ha eliminato: -
ha eliminato:

594 6 Discussion

596 6.1 FEM analysis at increasing geological detail

597 This study highlights some important features of crustal stress distribution on changing the geological
598 and geophysical constraints as input conditions (Spica et al., 2014, 2017; Massaro et al., 2018).

599 Although the results have to be considered as a first-order approximation, the changes in stress
600 distribution are appreciable and useful for a better understanding of the limitations and advantages of
601 FEM.

602 Under the assumptions of plane strain and gravitational loading, the use of homogeneous or non-
603 homogeneous lithology provides negligible effects in stress intensity and pattern (Fig. 4). This is likely

Formattato: SpazioDopo: 10 pt, Controlla righe isolate
ha eliminato: s

Formattato: SpazioDopo: 10 pt, Controlla righe isolate
ha eliminato: s
Formattato: Controlla righe isolate
ha eliminato: at

ha eliminato:
ha eliminato: FEM
ha eliminato:
ha eliminato: t

616 due to the limited thickness of the shallow units (Units FC, VD and, GF; Table 2) in the simulated
617 domain, which the results of which are dominated by Unit B (Table 2). However, this does not mean
618 that the influence of the upper units may be still negligible using smaller scales of the simulated domain.

619 Analysing the single magma chamber model outputs, it emerges how ΔP_e limits the effects of
620 gravitational loading. On the contrary, the dual magma chamber geometry better describes the inflation
621 induced by ΔP_e within magma chambers, with the formation of the stress arch in the σ_3 plot. It is
622 worth noting that for both single and dual magma chamber models, changing ΔP_e from 10 to 20 MPa
623 slightly affects the magnitude of the stress but not its general pattern (Appendices 1 and 2).

624 The presence of dykes in the magma feeding system dramatically changes the σ_3 and σ_1 patterns (Fig. 6),
625 which become quite homogeneous throughout the computational domain, with the only exception of
626 sidewall effects induced by the zero displacement conditions.

627 The addition of extensional field stress of 5 MPa reduces the sidewall effects and produces an almost
628 homogeneous stress distribution in the upper part of the computational domain, above the top of the
629 deep magma chamber. This, along with the additional inclusion of the damage zones introduced to
630 mimic the effects of CR faults, describes a volcanic system close to equilibrium, in which pressure
631 within the volcano feeding system almost equilibrates the lithostatic stress (Sulpizio et al., 2016).

633 6.2 Some implications of the stress state of the CVC inferred from FEM

634 The results from the most complete FEM runs highlight an almost homogeneous stress distribution in
635 the CVC area. This means the dual magma chamber model and the application of far-field stress
636 provide a stable geometry, which limits the stress changes to a few MPa. The majority of stress
637 variations are located at the tips of the magma chambers, as expected for pressurized or under-
638 pressurized cavities in the lithosphere (Martí and Geyer, 2009), implying that the whole feeding system
639 is in a quasi-equilibrium state. Even if we consider the scenario of complete emptying of the upper
640 conduit and part of the shallow magma chamber, as occurred occasionally during the past sub-Plinian

ha eliminato: the

ha eliminato: ed

ha formattato: Tipo di carattere: Non Corsivo

ha eliminato: the

ha formattato: Tipo di carattere: Non Corsivo

ha formattato: Tipo di carattere: 12 pt

ha eliminato:

ha eliminato: the

ha formattato: Tipo di carattere: Non Corsivo

ha eliminato: change

ha eliminato: x

ha eliminato: -

ha eliminato: .

ha formattato: Tipo di carattere: 12 pt

ha formattato: Tipo di carattere: 12 pt

ha formattato: Non Apice / Pedice

ha eliminato: volcanic system

ha eliminato:

Formattato: SpazioDopo: 10 pt, Controlla righe isolate

Formattato: SpazioDopo: 0 pt, Controlla righe isolate

ha eliminato: the

ha eliminato:

ha eliminato: i

ha eliminato: occurred

656 and Plinian eruptions (Luhr et al., 2002; Saucedo et al., 2010; Massaro et al., 2018), this would result
 657 in the restoration of the stress arch, which is still a stable stress configuration. Even complete emptying
 658 of the shallow magma chamber would probably be ineffective for triggering a large collapse (caldera-
 659 forming) of the feeding system.
 660 Beside and beyond the limitations due to the first-order approximation of the FEM analysis, other
 661 sources of uncertainty in the discussion about the present and future stress state of the CVC come from
 662 not considering gravity-driven processes, such as volcano spreading due to plastic deformation of Unit
 663 GF (Norini et al., 2010, 2019) and detailed regional tectonics (Norini et al., 2010, 2019). The effect of
 664 the two fault systems bordering the CR is here simulated by degrading the mechanic properties of rocks
 665 in an area of about 1 km width up to a depth of 10 km. Although the effects are negligible at the scale
 666 of the computational domain, it cannot be excluded that some local significant effects that cannot be
 667 resolved using the described approach.

669 7 Summary and conclusion

670 The presented study highlights the importance of using complete and detailed geological and
 671 geophysical data when dealing with FEM of volcanic areas. The different geological detail used in the
 672 model runs showed how the stress pattern depends critically on the geometry of the volcano feeding
 673 system, with huge differences in having a single or double magma chamber system and, in particular,
 674 whether or not the magma chamber(s) are connected to the surface by feeder dykes and conduits. The
 675 geometry of the feeding system is prevalent on model outputs with respect to varying rock properties
 676 (i.e. Young modulus) of one order of magnitude. In the case of CVC, the use of subsurface
 677 homogeneous or stratified lithology does not influence the FEM outputs much, the subsurface geology
 678 of the computational domain being dominated by carbonates (Unit B).

ha eliminato: the

ha eliminato: probably

ha eliminato:

ha eliminato:

Formattato: SpazioDopo: 6 pt, Controlla righe isolate

ha eliminato:

ha eliminato: ies

ha eliminato: the GF

ha eliminato: are

Formattato: SpazioDopo: 10 pt, Controlla righe isolate

ha eliminato: ed

ha eliminato: t

ha eliminato: e

ha eliminato: depends

ha eliminato: if

ha eliminato: or not

ha eliminato: much

ha eliminato: being

ha eliminato:

696 Beside and beyond the results obtained by analysing the influence of detailed geological and
 697 geophysical data, the presented modelling confirms the close to equilibrium state of the volcano, which
 698 is the expected stress distribution induced by a feeding system directly connected to the surface,
 699 The Complete emptying of the upper conduit and part of the shallow magma chamber, as occurred
 700 occasionally in the past, originating sub-Plinian and Plinian eruptions, would result in restoration of
 701 the stress arch, which is still a stable stress configuration. It follows that large magnitude, caldera-
 702 forming eruptions are possible only if the bigger deep magma chamber is also involved and
 703 significantly emptied during an eruption.

ha eliminato:

Formattato: SpazioDopo: 0 pt, Controlla righe isolate

ha eliminato: occurred

ha eliminato: the

ha eliminato:

ha eliminato:

705 **Tables**

707 **Table 1 - Element types used in LISA analysis considering the final conduit feeding system**
 708 **configuration – Fig.1d, panel vi)**

<i>E-W cross-section (a-a')</i>	Element Type	Elements	Nodes
FC Fuego de Colima	quad4-tri3	372	384
VD Volcanic Deposits	quad4-tri3	245	273
GF Graben Fill	quad4-tri3	456	338
B Basament	quad4-tri3	3088	2907
CG Colima graben	quad4-tri3	48	71

715 **Total Elements: 4209**

717 **Table 2 - Rock mass and mechanical properties of the geological Units used in the finite-element model**
 718 **(from Norini et al., 2010, 2019).**

<u>Acronym</u>	<u>Model Unit</u>	<u>Rock Type</u>	<u>Density (kg/m³)</u>	<u>Young's Modulus (MPa)</u>	<u>Poisson's ratio ν</u>
FC	Fuego de Colima	Andesitic lavas and pyroclastic deposits forming the Paleofuego-Fuego de Colima volcano	2242	1.4×10^3	0.30

VD	Volcaniclastic deposits	Pyroclastic and epiclastic deposits covering the southern flank of the CVC	1539	1.7×10^3	0.32
GF	Graben Fill	Quaternary alluvial, colluvial, lacustrine deposits filling the graben	1834	1.5×10^3	0.35
B	Basement	Cretaceous limestones and intrusive rocks forming the bed-rock underlying the CVC	2650	3.6×10^4	0.30

725

726

727

728 Appendices

729

730 Appendix 1

731 E-W gravitational modelling of the CVC domain (stratified lithology) for all configurations
 732 investigated. The magnitude and pattern of the principal stress account for a) single magma chamber
 733 model (4426 nodes: 4426); b) dual magma chamber model (number of nodes: 4161 nodes); c) dual
 734 magma chamber with conduits model (number of nodes: 3737 nodes). The Dimensions of the deep
 735 magma chamber: $2a = 14$ km and $2b = 3.6$ km at 15 km of depth; shallow magma chamber: $2a = 3.5$
 736 km and $2b = 2$ km at 6 km. ΔP_e and ΔP_o equal to= 20 MPa for the deep chamber, and 5 MPa for the
 737 shallower. Black dotted lines highlight the passage from different stress values. Note that the scales of
 738 stress values are different for each panel in order to maximize the simulation details.

739

740 Appendix 2

741 E-W gravitational modelling of the CVC domain (stratified lithology) considering an extensional far
 742 field of 5 MPa for all configurations investigated. The magnitude and pattern of the principal stress
 743 account for a) single magma chamber model (nodes: 4426 nodes); b) dual magma chamber model
 744 (number of nodes: 4161 nodes); c) dual magma chamber with conduits model (number of elements:
 745 3737 nodes). The Dimensions of the deep magma chamber: $2a = 14$ km and $2b = 3.6$ km at 15 km
 746 depth; shallow magma chamber: $2a = 3.5$ km and $2b = 2$ km at 6 km. ΔP_e and ΔP_o are equal to= 20
 747 MPa for the deep chamber, and 5 MPa for the shallower. Black dotted lines highlight the passage from
 748 different stress values. The Red arrows indicate the direction of the applied far-field stress. Note that
 749 the scales of stress values are different for each panel in order to maximize the simulation details.

750

751 Figure Captions

752

Formattato: Controlla righe isolate

ha eliminato:

Formattato: Controlla righe isolate

Formattato: Interlinea: multipla 1,15 ri, Controlla righe isolate

ha eliminato: -

ha eliminato: number of

ha formattato: Tipo di carattere: Non Corsivo

ha formattato: Tipo di carattere: 12 pt, Non Corsivo

ha formattato: Tipo di carattere: Non Corsivo

ha eliminato: are

ha formattato: Tipo di carattere: Non Corsivo

Formattato: Controlla righe isolate

Formattato: Interlinea: multipla 1,15 ri, Controlla righe isolate

ha eliminato: -

ha eliminato: -

ha eliminato: number of

ha eliminato: of

ha formattato: Tipo di carattere: Non Corsivo

ha formattato: Tipo di carattere: Non Corsivo

ha eliminato: $2b$

Formattato: Controlla righe isolate

ha eliminato: s

763 **Fig. 1** (a) Morphotectonic map of the Colima Volcanic Complex (NC = Nevado de Colima volcano;
 764 FC = Fuego de Colima volcano) and Colima Rift with the main tectonic and volcano-tectonic structures
 765 (NCG = Northern Colima Graben; CCG = Central Colima Graben, from Norini et al., 2019). Inset, the
 766 location of the Colima Volcanic Complex (CVC) within the Trans-Mexican Volcanic Belt (TMVB) is
 767 shown in the frame of the subduction-type geodynamic setting of Central America (from Davila et al.,
 768 2019); (b) general sketch of the geometrical configurations used in LISA; (c) example of mesh of the
 769 investigated area for the dual magma chamber model with conduits (case v in panel (b), considering
 770 zero displacement along the bottom and left and right sides. Note that for case (vi) in panel (b) the zero
 771 displacement is removed from the lateral sides; (d) sketch of the Fuego de Colima feeding system
 772 composed of a 15 km-deep magma chamber connected to the surface via a 6 km-deep magma chamber
 773 and dykes. ΔP_{chs} and ΔP_{chd} indicate either excess or over pressure (depending on the model used) in
 774 the shallow and deep chambers, respectively (modified from Massaro et al., 2019).

775

776 **Fig. 2** Results of the sensitivity analysis carried out on the Young modulus variations within each rock
 777 layer of the domain considering different configurations (stratified substratum model – 4426
 778 nodes; single magma chamber model – 4426 nodes; dual magma chamber model – 4161
 779 nodes; dual magma chamber with conduits model – 3737 nodes; 3737). For each geological unit
 780 (B, FC, GF, VD), the relative global variation in L_2 (%) is provided for σ_1 and σ_3 . The $x(-)$ and $x(+)$
 781 vectors indicate the variation in Young's modulus variation by an order of magnitude with respect to
 782 the x_{ref} vector, containing the stress values calculated by using the values of the material's properties
 783 indicated in Table 2.

784

785 **Fig. 3** Spatial variation (%) of the L_2 norm's components at varying Young modulus for selected cases
 786 of Units B and VD: (a) Unit B in the stratified substratum model (4426 nodes); (b) Unit B in the single
 787 magma chamber model (4426 nodes); (c) Unit B in the dual magma chamber model (4161 nodes);
 788 (d) Unit VD in the dual magma chamber with conduits model (nodes: 3737 nodes). Symbols $x(-)$ ($-$)
 789 and $x(+)$ have the same meaning as inof Figure 2.

790

791 **Fig. 4** E-W gravitational modelling of the CVC domain. The scale of the mesh is expressed in units of
 792 design (1 UD = 1 km). The domain extends 60 km along the x -axis, and 30 km along the z -axis. The
 793 number of nodes used in the mesh is set to 4426. The magnitude and pattern of the principal stresses
 794 (dotted black lines) are reported for (a) homogeneous stratigraphy (Unit FC = andesitic lavas and
 795 pyroclastic deposits) and (b) non-homogeneous stratigraphy (Unit FC; Unit B = Cretaceous limestone
 796 and intrusive rocks forming the bedrock underlying the CVC; Unit GF = Quaternary alluvial, colluvial
 797 and lacustrine deposits filling the graben; Unit VD = volcanoclastic deposits covering the southern flank
 798 of the CVC). The blue line contours the unperturbed part of the domain, which extends ca. 30 km
 799 horizontally and ca. 25 km vertically. Note that the scale of stress values is the same for all simulations.

800

Formattato: Interlinea: multipla 1,15 ri, Controlla righe isolate

ha eliminato: the in

ha eliminato: ,

ha eliminato: -

ha eliminato: -

ha formattato: Tipo di carattere: Non Corsivo

ha formattato: Tipo di carattere: 10 pt

ha formattato: Tipo di carattere: Non Corsivo

ha formattato: Tipo di carattere: 10 pt

Formattato: SpazioDopo: 12 pt, Interlinea: multipla 1,15 ri

ha eliminato: :

Formattato: SpazioDopo: 12 pt, Interlinea: multipla 1,15 ri

ha formattato: Tipo di carattere: 10 pt

ha formattato: Tipo di carattere: Non Corsivo

ha eliminato: : 4426

ha eliminato: : 4426

ha eliminato: nodes:

ha eliminato:)

ha eliminato:

Formattato: SpazioDopo: 12 pt, Interlinea: multipla 1,15 ri, Controlla righe isolate

ha eliminato:

ha eliminato: -

ha eliminato: the

ha formattato: Tipo di carattere: Non Corsivo

ha eliminato: for

ha eliminato: the

ha eliminato: t

ha eliminato: s

ha eliminato: -

ha eliminato: ,

ha formattato: Tipo di carattere: Non Corsivo

ha eliminato: the

ha eliminato:

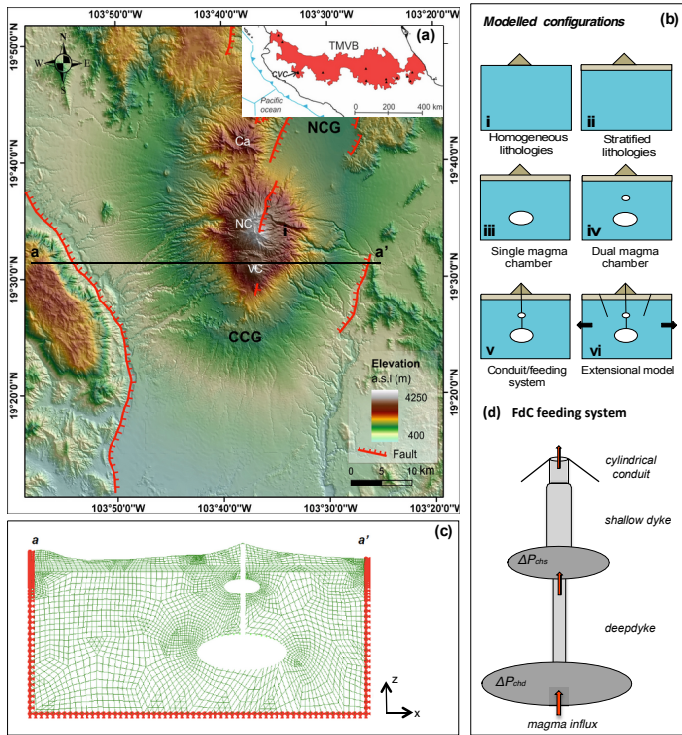
822 **Fig. 5** E-W gravitational modelling of the CVC domain with non-homogeneous stratigraphy. The
 823 magnitude and pattern of the principal stresses are reported for (a) the single magma chamber model
 824 represented by a magma chamber ($2a = 14$ km and $2b = 3.6$ km) at 15 km depth, and (b) the dual
 825 magma chamber model composed of a 15 km-deep magma chamber ($2a = 14$ km and $2b = 3.6$ km) and
 826 a shallow 6 km-deep one ($2a = 3.5$ km and $2b = 2$ km). The magma chambers are not connected. ΔP_0
 827 is set to 10 and 5 MPa for the 15 km-deep and 6 km-deep magma chambers, respectively. The number
 828 of nodes is set to 4426 and 4161 for the single and dual magma chamber models, respectively. Black
 829 dotted lines highlight the passage from different stress values. The red dotted line in panel (b) indicates
 830 the formation of the stress arch. Note that the scale of stress values is different for each panel in order
 831 to maximize the simulation details.
 832

833 **Fig. 6** E-W gravitational modelling of the CVC domain with non-homogeneous stratigraphy
 834 accounting for a dual magma chamber system connected by dykes via the surface (deep magma
 835 chamber, $2a = 14$ km and $2b = 3.6$ km at 15 km depth; shallow magma chamber, $2a = 3.5$ km and $2b =$
 836 $= 2$ km at 6 km depth). The magnitude and pattern of the principal stresses are shown. The number
 837 of nodes used is set to 3737. ΔP_0 is set to 10 and 5 MPa for the 15 km-deep and 6 km-deep magma
 838 chambers, respectively. The black dotted lines in panel (ii) highlight the passage from different stress
 839 values. Note that the scale of stress values are is different for each panel in order to maximize the
 840 simulation details.
 841

842 **Fig. 7** E-W gravitational modelling of the CVC domain with non-homogeneous stratigraphy
 843 considering the extensional field stress. The magnitude and pattern of the principal stresses are shown
 844 for the single magma chamber model (panels i and -ii), the dual magma chamber model (panels iii and
 845 -iv) and, the dual magma chamber with conduits model (panels v-vi-vii--viii). Note that in panels vii
 846 and -viii the faults bordering the CG are shown. For all configurations, an extensive far-field stress of
 847 5 MPa is applied at the lateral boundaries of the domain. In panels vii and -viii, the additional effect of
 848 the local extensive field is simulated using a reduced values of material properties (Table 2). ΔP_0 is set
 849 to 10 and 5 MPa for the 15 km-deep and 6 km-deep magma chambers, respectively. Black dotted lines
 850 highlight the passage from different stress values. The red arrows indicate the direction of the applied
 851 far- field stress. Note that the scale of stress values is different for each panel in order to maximize the
 852 simulation details.
 853

854 [Figure 1](#)

- ha eliminato: ¶
- ha eliminato: a
- Formattato: SpazioDopo: 0 pt, Interlinea: multipla 1,15 ri, Controlla righe isolate
- ha eliminato: -
- ha eliminato: t
- ha eliminato: of
- ha formattato: Tipo di carattere: Non Corsivo
- ha formattato: Tipo di carattere: Non Corsivo
- ha formattato: Tipo di carattere: Non Corsivo
- ha formattato: Tipo di carattere: Non Corsivo
- ha eliminato: -
- ha eliminato: are
- Formattato: Interlinea: multipla 1,15 ri, Controlla righe isolate
- ha eliminato: -
- ha eliminato: a
- ha eliminato: t
- ha eliminato: ed
- ha eliminato: of
- ha formattato: Tipo di carattere: Non Corsivo
- ha formattato: Tipo di carattere: Non Corsivo
- ha eliminato: 2b
- Formattato: Interlinea: multipla 1,15 ri, Controlla righe isolate
- ha eliminato: -
- ha eliminato: a
- ha eliminato: t
- ha eliminato: i



872

873

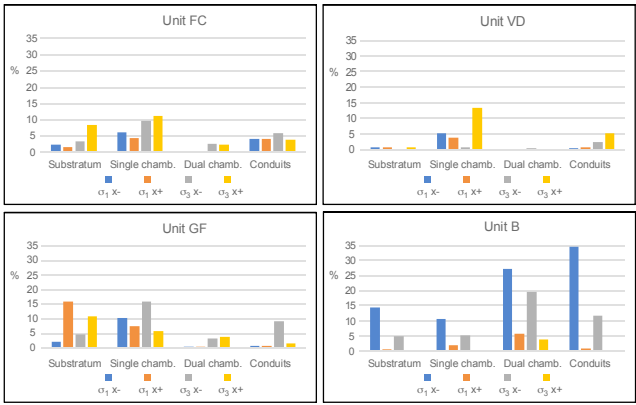
874

875

876

877

878 [Figure 2](#)



879

880

881

882

883

884

885

886

887

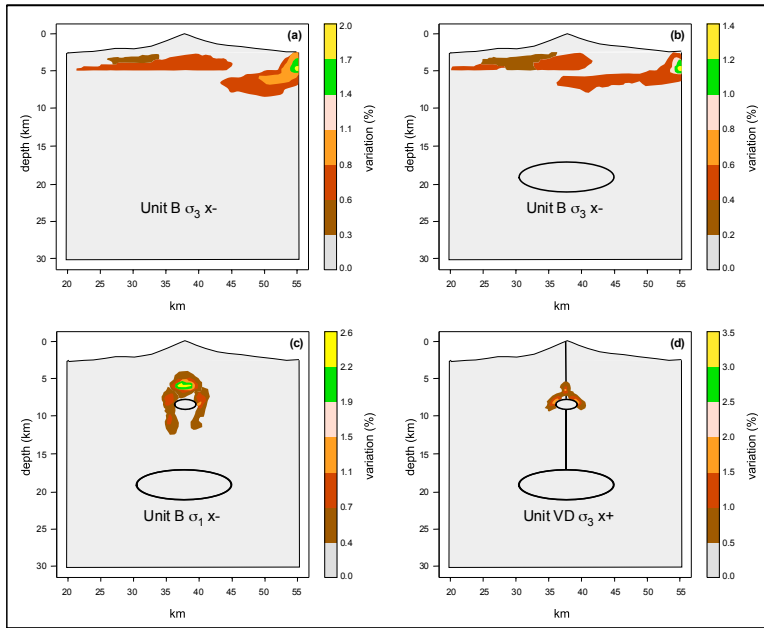
888

889

890

891

892 [Figure 3](#)



893

894

895

896

897

898

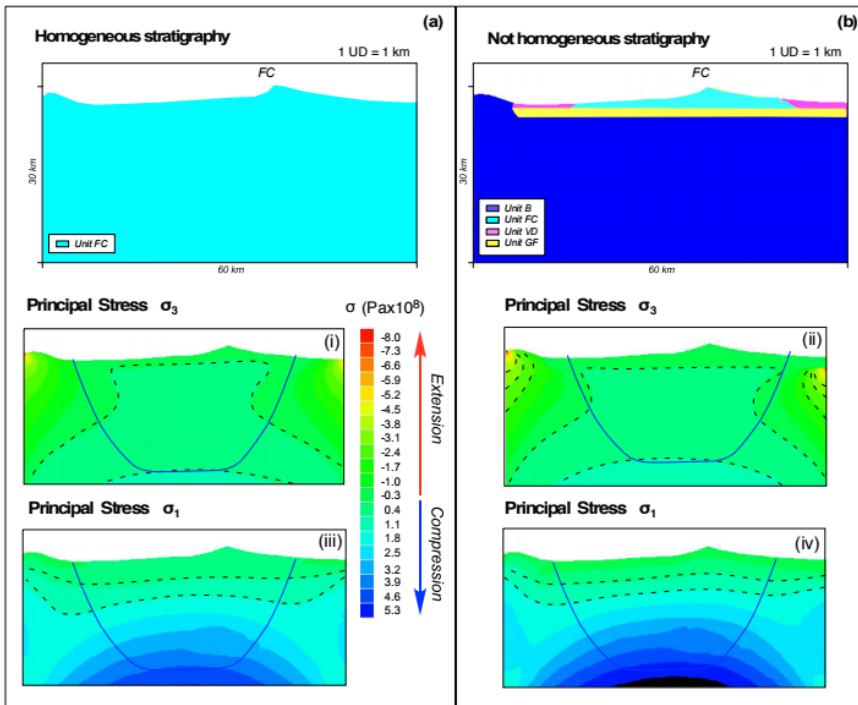
899

900

901

902 [Figure 4](#)

903



904

905

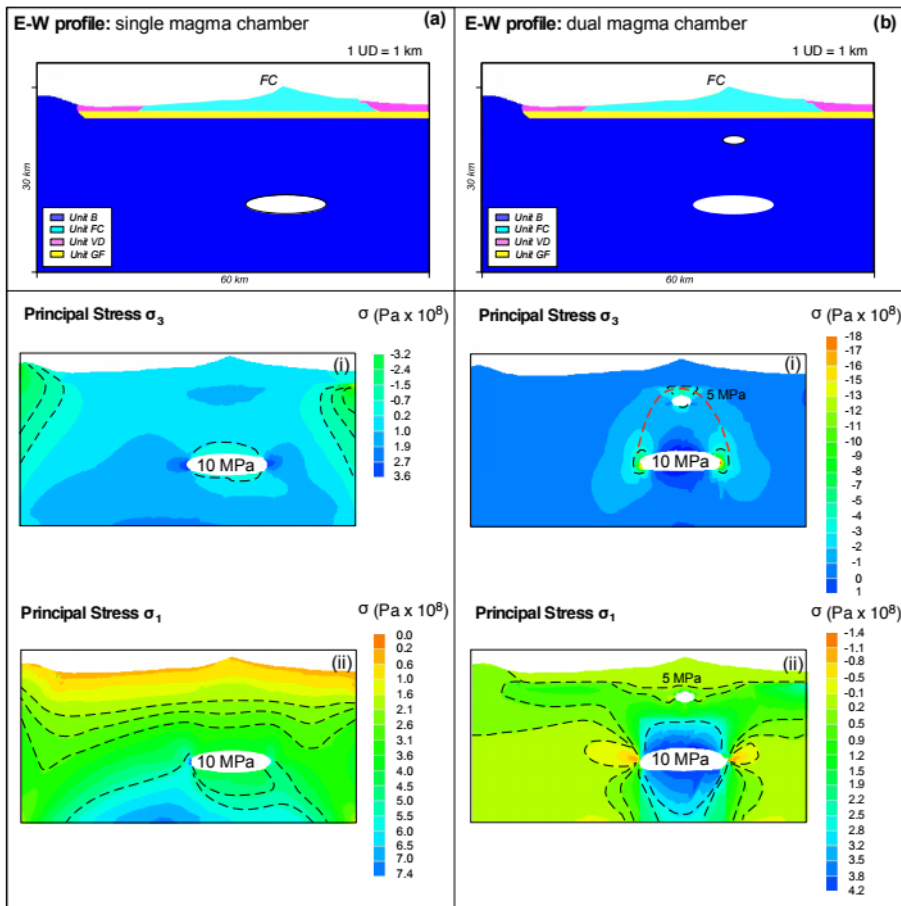
906

907

908

909

910 [Figure 5](#)



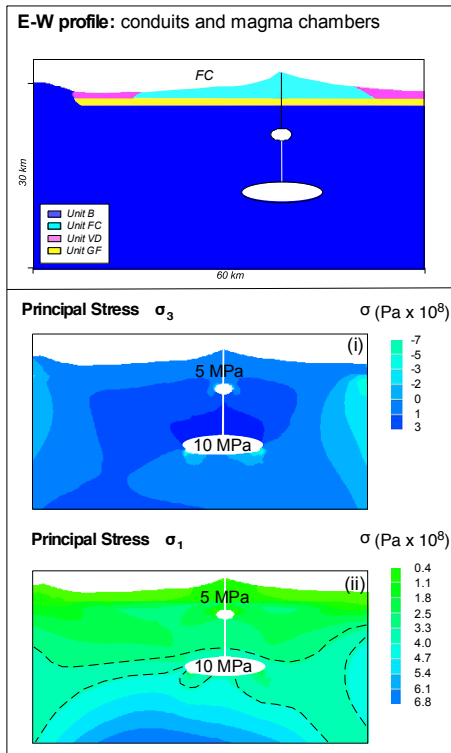
911

912

913

914

915 [Figure 6](#)



916

917

918

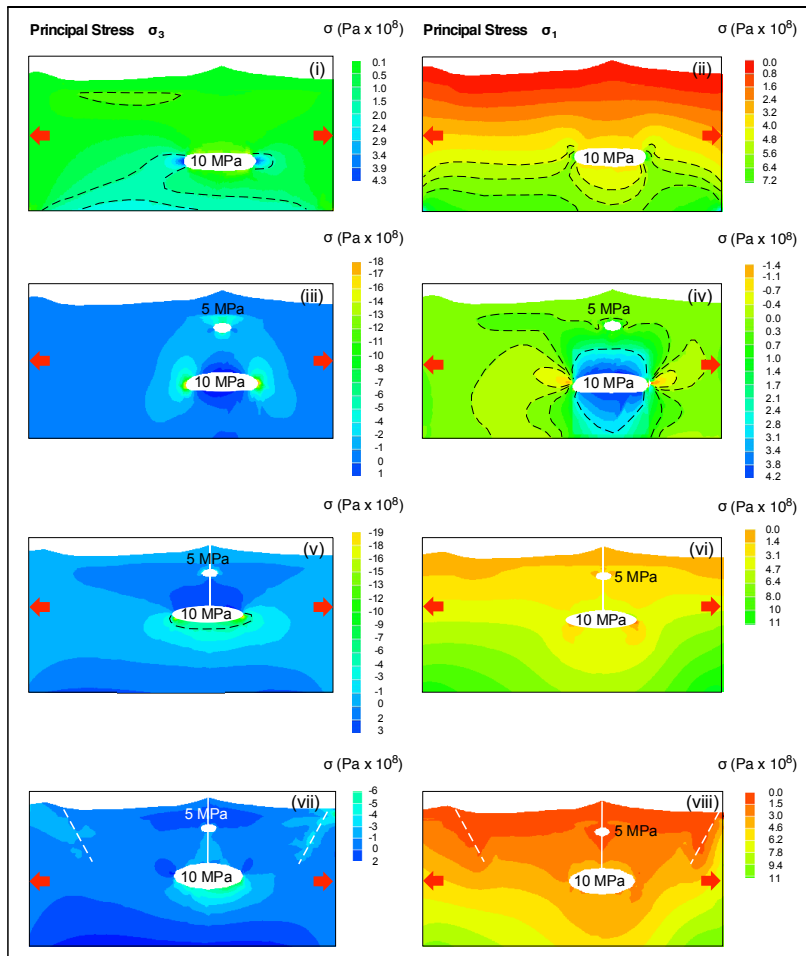
919

920

921

922

923 [Figure 7](#)



924

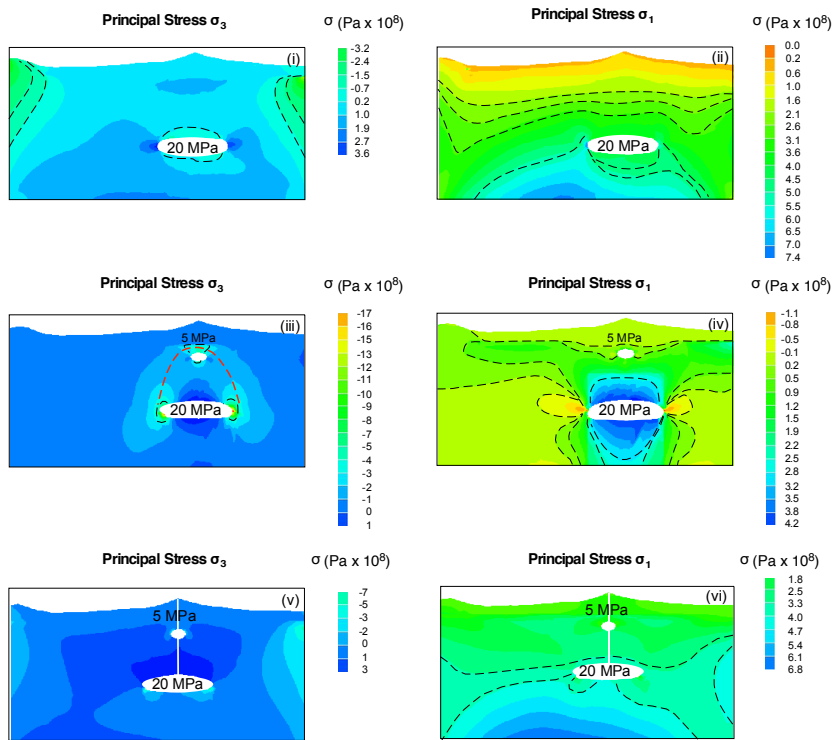
925

926

927

928 [Appendix 1](#)

Appendix 1



929

930

931

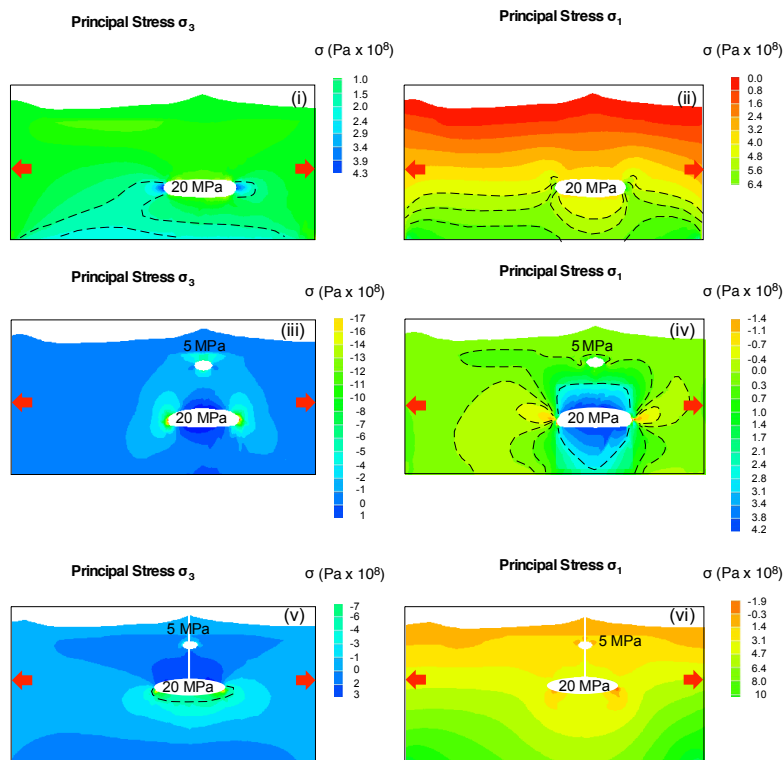
932

933

934

935 [Appendix 2](#)

Appendix 2



936

937

938 Code/Data Availability

939 The LISA code is available at <https://lisafea.com/>.

940

941 Author's contribution

942 SM, RS, AC, GN and GG conceived the study. SM and RS wrote the bulk of the manuscript with the
943 input of all the co-authors. SM and GL compiled the numerical simulations and formulated the adopted
944 methodology. MP and SM carried out the sensitivity analysis. All authors worked on the interpretation

945 [of the results.](#)

946

947 [Competing interests:](#) The authors declare that they have no conflict of interest.

948

949 [Acknowledgements:](#) The manuscript received a professional copy-editing. SM thanks the LISA
950 customer service for the support received. In particular, Karl.

951

952 [References](#)

953 [Albino, F., Pinel, V., and Sigmundsson, F., 2010. Influence of surface load variations on eruption
954 likelihood: application to two Icelandic subglacial volcanoes, Grímsvötn and Katla. Geophysical
955 journal international, 181\(3\), 1510-1524.](#)

956 [Albino, F., Amelung, F., and Gregg, P., 2018. The role of pore fluid pressure on the failure of magma
957 reservoirs: insights from Indonesian and Aleutian arc volcanoes. Journal of Geophysical Research:
958 Solid Earth, 123\(2\), 1328-1349.](#)

959 [Anderson E.M., 1936. The dynamics of formation of cone sheets, ring dykes and cauldron
960 subsidence. Proc R Soc Edinburgh 56:128–163.](#)

961 [Allan, J.F., 1985. Sediment depth in the NCG from 3-D interpretation of gravity. Geofis. Int. 24, 21–
962 30 \(1985\).](#)

963 [Allan, J.F. 1986. Geology of the Northern Colima and Zacoalco grabens, Southwest Mexico: Late
964 Cenozoic rifting in the Mexican Volcanic Belt. Geol. Soc. Am. Bull. 97, 473–485](#)

965 [Allan, J.F., Nelson, S.A., Luhr, J.F., Charnichael, I.S.E., Wopat, M., Wallace, P.J., 1991: Pliocene-
966 Holocene rifting and associated volcanism in Southwest Mexico: an exotic terrane in the making. In:
967 Dauphin, J.P., Simoneit, R.R.T. \(eds.\) The Gulf and Peninsular Provinces of the Californias, AAPG
968 Mem., vol. 47, pp. 425–445.](#)

969 [Andrew, R.E., and Gudmundsson, A., 2008. Volcanoes as elastic inclusions: Their effects on the
970 propagation of dykes, volcanic fissures, and volcanic zones in Iceland. Journal of Volcanology and
971 Geothermal Research, 177\(4\), 1045-1054.](#)

972 [Arámbula-Mendoza, R., Reyes-Dávila, G., Dulce, M.V.B., González-Amezcuca, M., Navarro- Ochoa,
973 C., Martínez-Fierros, A., and Ramírez-Vázquez, A., 2018. Seismic monitoring of effusive-explosive
974 activity and large lava dome collapses during 2013–2015 at Volcán de Colima, Mexico. J. Volcanol.
975 Geotherm. Res., 351, 75-88.](#)

976 [Babuška, I., Ihlenburg, F., Paik, E. T., and Sauter, S.A., 1995. A generalized finite element method
977 for solving the Helmholtz equation in two dimensions with minimal pollution. Computer methods in
978 applied mechanics and engineering, 128\(3-4\), 325-359.](#)

979 [Bandy, W.L., Mortera-Gutiérrez, C.A., Urrutia- Fucugauchi, J., Hilde, T.W.C. 1995. The subducted
980 Rivera-Cocos plate boundary: where is it, what is it, and what is its relationship to the Colima Rift?
981
982
983
984
985](#)

986 [Geophys. Res. Lett.](#) **22**, 3075–3078.

987 [Barrier, B., Bourgois, J., Michaud, F., 1990: The active Jalisco triple junction rift system. C.R. Acad.](#)
988 [Sci. Paris](#), 310 (II), 1513–1520.

989 [Bathe, K. J., Zhang, H., and Ji, S., 1999. Finite element analysis of fluid flows fully coupled with](#)
990 [structural interactions. Computers and Structures](#), 72(1-3), 1-16.

991

992 [Bonafede, M., Parenti, B., Rivalta, E., 2002. On strike-slip faulting in layered media. Geophysical](#)
993 [Journal International](#), 149(3), 698-723.

994

995 [Bonasia R, Capra L, Costa A, Macedonio G, Saucedo R., 2011. Tephra fallout hazard assessment for](#)
996 [a Plinian eruption scenario at Volcan de Colima. J Volcanol Geotherm Res](#) 203: 12–22.

997

998 [Boresi, A.P., Schmidt, R.J., and Sidebottom, O.M., 1985. Advanced mechanics of materials \(Vol. 6\).](#)
999 [New York et al.: Wiley.](#)

1000

1001 [Buchmann T. and Conolly P.T., 2007. Contemporary kinematics of the Upper Rhine Graben: A 3D](#)
1002 [finite element approach. Global and Planetary Change](#) 58, 287–309.

1003

1004 [Bunney, 2014. The Effects of Structural Heterogeneities and In-elastic Rheology on Ground](#)
1005 [Deformation at Campi Flegrei Caldera, Italy. PhD Thesis.](#)

1006

1007 [Cabaniss, H.E., Gregg, P. M., and Grosfils, E.B., 2018. The role of tectonic stress in triggering large](#)
1008 [silicic caldera eruptions. Geophysical Research Letters](#), 45, 3889–3895. <https://doi.org/10.1029/2018GL077393>.

1009

1010 [Cayol, V., and Cornet, F. H., 1998. Effects of topography on the interpretation of the deformation field](#)
1011 [of prominent volcanoes: Application to Etna. Geophysical Research Letters](#), 25(11), 1979–1982.
1012 <https://doi.org/10.1029/98GL51512>.

1013

1014 [Cailleau, B., T.R. Walter, P. Janle, and E. Hauber, 2003. Modeling volcanic deformation in a regional](#)
1015 [stress field: Implications for the formation of graben structures on Alba Patera, Mars. J. Geophys.](#)
1016 [Res.](#), 108(E12), 5141, doi:10.1029/2003JE002135.

1017

1018 [Cailleau B., Thomas R, Walter, Peter Janle, Ernst Hauber, 2005. Unveiling the origin of radial grabens](#)
1019 [on Alba Patera volcano by finite element modelling Icarus](#) 176, 44–56.

1020

1021 [Cabrera-Gutiérrez, R., and Espíndola, J.M., 2010. The 1998-1999 eruption of Volcán de Colima,](#)
1022 [Mexico: an application of Maeda's viscoelastic model. Geofísica internacional](#), 49(2), 83-96.

1023

1024

1025 [Canales, J.P., Nedimović, M.R., Kent, G.M., Carbotte, S.M., and Detrick, R.S., 2009. Seismic](#)
1026 [reflection images of a near-axis melt sill within the lower crust at the Juan de Fuca ridge. Nature](#),
1027 [460\(7251\), 89.](#)

1028

1029 [Capra L., and Macías, J.L., 2002. The cohesive Naranjo debris-flow deposit \(10 km³\): A dam breakout](#)
1030 [flow derived from the Pleistocene debris-avalanche deposit of Nevado de Colima Volcano \(México\).](#)
1031 [Journal of Volcanology and Geothermal Research](#), 117(1-2), 213-235.

1032 [volume, J Volcanol Geotherm Res 310: 39-49.](#)

1033

1034 [Cianetti, S., Giunchi, C., and Casarotti, E., 2012. Volcanic deformation and flank instability due to](#)

1035 [magmatic sources and frictional rheology: the case of Mount Etna. Geophysical Journal International,](#)

1036 [191\(3\), 939-953.](#)

1037

1038 [Charco, M., and Galán del Sastre, P., 2014. Efficient inversion of three-dimensional finite element](#)

1039 [models of volcano deformation. Geophysical Journal International, 196\(3\), 1441-1454.](#)

1040

1041 [Chaput, M., Pinel, V., Famin, V., Michon, L., and Froger, J.L., 2014. Cointrusive shear displacement](#)

1042 [by sill intrusion in a detachment: A numerical approach. Geophysical Research Letters, 41\(6\), 1937-](#)

1043 [1943.](#)

1044

1045 [Cortés, A., 2005. Carta geológica del complejo volcánico de Colima. UNAM, Instituto de Geología.](#)

1046

1047 [Cortés, A., Garduño, V.H., Macías, J. L., Navarro-Ochoa, C., Komorowski, J.C., Saucedo, R., and](#)

1048 [Gavilanes, J. C. \(2010\). Geologic mapping of the Colima volcanic complex \(Mexico\) and implications](#)

1049 [for hazard assessment. Geol Soc Am Spec Pap, 464, 249-264.](#)

1050

1051 [Cortés, A., Komorowski, J. C., Macías, J. L., Capra, L., and Layer, P. W., 2019. Late Pleistocene-](#)

1052 [Holocene debris avalanche deposits from Volcán de Colima, Mexico. In Volcán de Colima \(pp. 55-](#)

1053 [79\). Springer, Berlin, Heidelberg.](#)

1054

1055 [Costa, A., Sparks, R.S.J., Macedonio, G., and Melnik, O., 2009. Effects of wall-rock elasticity on](#)

1056 [magma flow in dykes during explosive eruptions. Earth and Planetary Science Letters, 288\(3-4\), 455-](#)

1057 [462.](#)

1058

1059 [Costa, A., Gottsmann, J., Melnik, O., and Sparks, R. S. J., 2011. A stress-controlled mechanism for the](#)

1060 [intensity of very large magnitude explosive eruptions. Earth and Planetary Science Letters, 310\(1-2\),](#)

1061 [161-166.](#)

1062

1063 [Currenti, G., Bonaccorso, A., Del Negro, C., Scandura, D., and Boschi, E., 2010. Elasto-plastic](#)

1064 [modeling of volcano ground deformation. Earth and Planetary Science Letters, 296\(3-4\), 311-318.](#)

1065

1066 [Currenti, G., and Williams, C.A., 2014. Numerical modeling of deformation and stress fields around a](#)

1067 [magma chamber: Constraints on failure conditions and rheology. Physics of the Earth and Planetary](#)

1068 [Interiors, 226, 14-27.](#)

1069

1070 [Dávila, N., Capra, L., Ferrés, D., Gavilanes-Ruiz, J. C., and Flores, P., 2019. Chronology of the 2014–](#)

1071 [2016 Eruptive Phase of Volcán de Colima and Volume Estimation of Associated Lava Flows and](#)

1072 [Pyroclastic Flows Based on Optical Multi-Sensors. Remote Sensing, 11\(10\), 1167.](#)

1073

1074 [Del Potro, R. and Hürlimann, M., 2008. Geotechnical classification and characterization of materials](#)

1075 [for stability analyses of large volcanic slopes. Eng. Geol. 98\(1\), 1–17.](#)

1076

1077 [Dieterich J.H., and R.W. Decker, 1975. Finite element modeling of surface deformation associated](#)

1078 [with volcanism, J. Geophys. Res., 80, 4094–4102.](#)

1079

1078 [Escudero, C.R., and Bandy, W.L., 2017: Ambient seismic noise tomography of the Colima Volcano](#)

1079 [Complex. Bull. Volcanol. 79, 13.](#)

1080 [Fernández, J., Tiampo, K. F., Jentzsch, G., Charco, M., and Rundle, J.B., 2001. Inflation or deflation?](#)
1081 [New results for Mayon Volcano applying elastic-gravitational modeling. *Geophysical Research Letters*,](#)
1082 [28\(12\), 2349-2352.](#)

1083

1084 [Ferrari, L., Rosas-Elguera, J., Márquez, A., Oyarzun, R., Doblás, M., and Verma, S.P., 1999. Alkalic](#)
1085 [\(ocean-island basalt type\) and calc-alkalic volcanism in the Mexican volcanic belt: A case for plume-](#)
1086 [related magmatism and propagating rifting at an active margin?: Comment and Reply. *Geology*, 27\(11\),](#)
1087 [1055-1056.](#)

1088

1089 [Folch, A., Fernández, J., Rundle, J.B., Martí, J., 2000. Ground deformation in a viscoelastic medium](#)
1090 [composed of a layer overlying a half-space: a comparison between point and extended sources.](#)
1091 [*Geophys. J. Int.* 140 \(1\), 37–50.](#)

1092 [Frey, H.M., Lange, R.A., Hall, C.M., Delgado-Granados, H., Carmichael, I.S.E., 2007. A Pliocene](#)
1093 [ignimbrite flare-up along the Tepic-Zacoalco rift: evidence for the initial stages of rifting between the](#)
1094 [Jalisco block \(Mexico\) and North America. *Geol. Soc. Am. Bull.* 119, 49–64.](#)
1095 [http://dx.doi.org/10.1130/B25950.1.](#)

1096 [Fujita, E., Kozono, T., Ueda, H., Kohno, Y., Yoshioka, S., Toda, N., and Ida, Y., 2013. Stress field](#)
1097 [change around the Mount Fuji volcano magma system caused by the Tohoku megathrust earthquake,](#)
1098 [Japan. *Bulletin of volcanology*, 75\(1\), 679.](#)

1099

1100 [Gabrieli, A., Wilson, L., and Lane, S., 2015. Volcano–tectonic interactions as triggers of volcanic](#)
1101 [eruptions. *Proceedings of the Geologists' Association*, 126\(6\), 675–682.](#)

1102

1103 [Garduño-Monroy, V.H., Saucedo-Girón, R., Jiménez, Z., Gavilanes-Ruiz, J.C., Cortés-Cortés, A.,](#)
1104 [Uribe-Cifuentes, R.M. 1998: La Falla Tamazula, límite suroccidental del Bloque Jalisco, y sus relaciones](#)
1105 [con el Complejo Volcánico de Colima, México. *Revista Mexicana de Ciencias Geológicas* 15\(2\), 132–](#)
1106 [144.](#)

1107 [Gelman, S.E., Deering, C.D., Gutierrez, F.J., and Bachmann, O., 2013. Evolution of the Taupo](#)
1108 [Volcanic Center, New Zealand: petrological and thermal constraints from the Omega dacite.](#)
1109 [*Contributions to Mineralogy and Petrology*, 166\(5\), 1355-1374.](#)

1110

1111 [Geyer, A., and Martí, J., 2009. Stress fields controlling the formation of nested and overlapping](#)
1112 [calderas: implications for the understanding of caldera unrest. *Journal of Volcanology and Geothermal*](#)
1113 [Research, 181\(3-4\), 185-195.](#)

1114

1115 [Geyer, A., and Gottsmann, J., 2010. The influence of mechanical stiffness on caldera deformation and](#)
1116 [implications for the 1971–1984 Rabaul uplift \(Papua New Guinea\). *Tectonophysics*, 483\(3-4\), 399–](#)
1117 [412.](#)

1118

1119 [Geyer, A., Martí, J., and Villaseñor, A., 2016. First-order estimate of the Canary Islands plate-scale](#)
1120 [stress field: Implications for volcanic hazard assessment. *Tectonophysics*, 679, 125-139.](#)

1121

1122 [Gerbault, M., Cappa, F., Hassani, R., 2012. Elasto-plastic and hydromechanical models of failure](#)
1123 [around an infinitely long magma chamber. *Geochem. Geophys. Geosyst.* 13, Q03009.](#)
1124 [http://dx.doi.org/10.1029/2011GC003917.](#)

1125 [Gerbault, M., Hassani, R., Lizama CN, Souche, A., 2018. Three-Dimensional Failure Patterns Around](#)
1126 [an Inflating Magmatic Chamber. *Geochemistry, Geophysics, Geosystems*. AGU and the Geochemical](#)
1127 [Society, In press.](#)

1128 [Geshi, N., Kusumoto, S., and Gudmundsson, A., 2012. Effects of mechanical layering of host rocks](#)
1129 [on dike growth and arrest. Journal of Volcanology and Geothermal Research, 223, 74-82.](#)
1130

1131 [Grosfils, E.B., 2007. Magma reservoir failure on the terres- trial planets: Assessing the importance of](#)
1132 [gravitational loading in simple elastic models. J. Volcanol. Geotherm. Res., 166, 47-75,](#)
1133 [doi:10.1016/j.jvolgeores.2007.06.007.](#)

1134 [Grosfils, E.B., McGovern, P. J., Gregg, P.M., Galgana, G.A., Hurwitz, D.M., Long, S.M., Chestler,](#)
1135 [S.R., 2015. Elastic models of magma reservoir mechanics: a key tool for investigating planetary](#)
1136 [volcanism. Geol. Soc. London, Spec. Pub., 401\(1\), 239-267.](#)

1137 [Gudmundsson, A., and Brenner, S.L., 2004. How mechanical layering affects local stresses, unrests,](#)
1138 [and eruptions of volcanoes. Geophysical Research Letters, 31\(16\).](#)
1139

1140 [Gudmundsson, A., 2006. How local stresses control magma-chamber ruptures, dyke injections, and](#)
1141 [eruptions in composite volcanoes. Earth-Sci.Rev., 79\(1-2\), 1-31.](#)

1142 [Gudmundsson, A., 2011. Rock fractures in geological processes. Cambridge University Press.](#)
1143

1144 [Gudmundsson, A., 2012. Strengths and strain energies of volcanic edifices: implications for](#)
1145 [eruptions, collapse calderas, and landslides. Natural Hazards and Earth System Sciences, 12\(7\),](#)
1146 [2241.](#)
1147

1148 [Goennermann and Taisne, 2015. Magma Transport in Dikes. The Encyclopedia of Volcanoes.](#)
1149 [http://dx.doi.org/10.1016/B978-0-12-385938-9.00010-9.](#)

1150 [Gottsmann, J., Folch, A., and Rymer, H., 2006. Unrest at Campi Flegrei: A contribution to the](#)
1151 [magmatic versus hydrothermal debate from inverse and finite element modeling. Journal of](#)
1152 [Geophysical Research: Solid Earth, 111\(B7\).](#)
1153

1154 [Gutiérrez, F., and Parada, M.A., 2010. Numerical modeling of time-dependent fluid dynamics and](#)
1155 [differentiation of a shallow basaltic magma chamber. Journal of Petrology, 51\(3\), 731-762.](#)
1156

1157 [Hautmann, S., Gottsmann, J., Sparks, R.S.J., Costa, A., Melnik, O., and Voight, B., 2009. Modelling](#)
1158 [ground deformation caused by oscillating overpressure in a dyke conduit at Soufrière Hills Volcano,](#)
1159 [Montserrat. Tectonophysics, 471\(1-2\), 87-95.](#)

1160 [Heap, M. J., Villeneuve, M., Albino, F., Farquharson, J. I., Brothelande, E., Amelung, F., and Baud,](#)
1161 [P., 2020. Towards more realistic values of elastic moduli for volcano modelling. Journal of](#)
1162 [Volcanology and Geothermal Research, 390, 106684.](#)
1163

1164 [Hickey, J., Gottsmann, J., and Mothes, P., 2015. Estimating volcanic deformation source](#)
1165 [parameters with a finite element inversion: The 2001-2002 unrest at Cotopaxi volcano, Ecuador. J.](#)
1166 [Geophys. Res. Solid Earth, 120, 1473-1486, doi:10.1002/2014JB011731.](#)

1167 [Hoek, E. and Brown, E.T, 1997. Practical estimates of rock mass strength. Int. J. Rock Mech. Min. Sci.](#)
1168 [34, 1165-1186.](#)

1169 [Holohan, E.P., Schöpfer, M. P. J., and Walsh, J.J., 2015. Stress evolution during caldera collapse.](#)
1170 [Earth and Planetary Science Letters, 421, 139-151.](#)

1171 [Huang, X., and Zhang, Z., 2012. Stress arch bunch and its formation mechanism in blocky stratified](#)
1172 [rock masses. Journal of Rock Mechanics and Geotechnical Engineering, 4\(1\), 19-27.](#)
1173
1174 [Karlstrom, L., Dufek, J., Manga, M., 2010. Magma chamber stability in arc and continental crust. J.](#)
1175 [Volcanol. Geotherm. Res. 190, 249–270.](#)
1176
1177 [Kinvig, H. S., Geyer, A., and Gottsmann, J., 2009. On the effect of crustal layering on ring-fault](#)
1178 [initiation and the formation of collapse calderas. Journal of Volcanology and Geothermal Research,](#)
1179 [186\(3-4\), 293-304.](#)
1180
1181 [Jaeger, J.C., Cook, N.G., and Zimmerman, R., 2009. Fundamentals of rock mechanics. John Wiley and](#)
1182 [Sons.](#)
1183
1184 [Jeanne, P., Guglielmi, Y., Rutqvist, J., Nussbaum, C., and Birkholzer, J., 2017. Field characterization](#)
1185 [of elastic properties across a fault zone reactivated by fluid injection. Journal of Geophysical Research:](#)
1186 [Solid Earth, 122\(8\), 6583-6598.](#)
1187
1188 [Jellinek, A.M. and DePaolo, D.J., 2003. A model for the origin of large silicic magma chambers:](#)
1189 [precursors of caldera-forming eruptions. Bull. Volcanol. 65, 363–381.](#)
1190
1191 [Lister, J.R. and Kerr, R.C., 1991. Fluid-mechanical models of crack propagation and their application](#)
1192 [to magma transport in dykes. Journal of Geophysical Research 96,10,049–10,077.](#)
1193
1194 [Long, S.M., and Grosfils, E.B., 2009. Modeling the effect of layered volcanic material on magma](#)
1195 [reservoir failure and associated deformation, with application to Long Valley caldera, California.](#)
1196 [Journal of Volcanology and Geothermal Research, 186\(3-4\), 349-360.](#)
1197
1198 [López-Loera, H., Urrutia-Fucugauchi, J., Alva-Valdivia, L., 2011. Estudio aeromagnético del complejo](#)
1199 [volcánico de Colima, occidente de México – implicaciones tectónicas y estructurales. Revista](#)
1200 [Mexicana de Ciencias Geológicas 28, 349–370.](#)
1201
1202 [Lungarini, L., Troise, C., Meo, M., and De Natale, G., 2005. Finite element modelling of topographic](#)
1203 [effects on elastic ground deformation at Mt. Etna. Journal of volcanology and geothermal research,](#)
1204 [144\(1-4\), 257-271.](#)
1205
1206 [Luhr, J.F., and Carmichael, I.S., 1985. Contemporaneous eruptions of calc-alkaline and alkaline](#)
1207 [magmas along the volcanic front of the Mexican Volcanic Belt. Geofísica Internacional, 24\(1\).](#)
1208
1209 [Luhr J.F., 2002. Petrology and geochemistry of the 1991 and 1998-1999 lava flows from Volcan Colima,](#)
1210 [Mexico. J Volcanol Geotherm Res 117: 169–194.](#)
1211
1212 [Maccaferri, F., Bonafede, M., and Rivalta, E., 2010. A numerical model of dyke propagation in layered](#)
1213 [elastic media. Geophysical Journal International, 180\(3\), 1107-1123.](#)
1214
1215 [Maccaferri, F., Bonafede, M., and Rivalta, E., 2011. A quantitative study of the mechanisms](#)
1216 [governing dike propagation, dike arrest and sill formation. Journal of Volcanology and Geothermal](#)
1217 [Research, 208\(1-2\), 39-50.](#)
1218

- 1219 [Maccaferri, F., Rivalta, E., Keir, D., and Acocella, V., 2014. Off-rift volcanism in rift zones](#)
1220 [determined by crustal unloading. *Nature Geoscience*, 7\(4\), 297-300.](#)
- 1221
- 1222 [Maccaferri, F., Smittarello, D., Pinel, V., and Cayol, V., 2019. On the propagation path of magma-](#)
1223 [filled dikes and hydrofractures: The competition between external stress, internal pressure, and crack](#)
1224 [length. *Geochemistry, Geophysics, Geosystems*, 20\(4\), 2064-2081.](#)
- 1225
- 1226 [Macías, J.L., Saucedo, R., Gavilanes, J.C., Varley, N., Velasco, García S., Bursik, M.I., Vargas,](#)
1227 [Gutiérrez V., Cortés, A., 2006. Flujos piroclásticos asociados a la activi- dad explosiva del Volcán de](#)
1228 [Colima y perspectivas futuras. *GEOS* 25\(3\), 340–351.](#)
- 1229 [Macías J, Arce J, Sosa G, Gardner JE, Saucedo R., 2017. Storage conditions and magma processes](#)
1230 [triggering the 1818CE Plinian eruption of Volcán de Colima. *J Volcanol GeothermRes*](#)
1231 [doi:10.1016/j.jvolgeores.2017.02.025.](#)
- 1232 [Macdonald, K.C., 1982. Mid-ocean ridges: fine scale tectonic, volcanic and hydrothermal pro- cesses](#)
1233 [within the plate boundary zone. *Annual Review of Earth and Planetary Sciences* 10, 155–190.](#)
- 1234 [MacLeod, C.J., Yaouancq, G., 2000. A fossil melt lens in the Oman ophiolite: implications for magma](#)
1235 [chamber processes at fast spreading ridges. *Earth and Planetary Science Letters* 176, 357–373.](#)
- 1236 [Manconi A., Walter TR, and Amelung, F., 2007. Effects of mechanical layering on volcano](#)
1237 [deformation. *Geophys. J. Int.* \(2007\) 170, 952–958.](#)
- 1238 [Manconi, A., Longpré, M.A., Walter, T.R., Troll, V.R., Hansteen, T.H., 2009. The effects of flank](#)
1239 [collapses on volcano plumbing systems. *Geology* 37 \(12\), 1099–1102.](#)
- 1240 [Marinos, P. and Hoek, E., 2000. GSI: a geologically friendly tool for rock mass strength estimation.](#)
1241 [In: *Proc. GeoEng2000 Conference*, Melbourne, 1422–1442.](#)
- 1242 [Martí, J., and Geyer, A., 2009. Central vs flank eruptions at Teide–Pico Viejo twin stratovolcanoes](#)
1243 [\(Tenerife, Canary Islands\). *Journal of Volcanology and Geothermal Research*, 181\(1-2\), 47-60.](#)
- 1244
- 1245 [Massaro S, Sulpizio R, Costa A, Capra L., Lucchi F., 2018. Understanding eruptive style variations at](#)
1246 [calc-alkaline volcanoes: the 1913 eruption of Fuego de Colima volcano \(Mexico\). *Bulletin of*](#)
1247 [Volcanology](#), 80:62.
- 1248 [Massaro, S., Costa, A., Sulpizio, R., Coppola, D., Capra, L., 2019. Cyclic activity of Fuego de Colima](#)
1249 [volcano \(Mexico\): insights from satellite thermal data and non-linear models. *Solid Earth*, 1429-1450.](#)
- 1250 [Margottini, C., Canuti, P., Sassa, K., 2013. *Landslide science and practice \(Vol. 1\)*. Berlin: Springer.](#)
- 1251
- 1252 [Masterlark, T., Feigl, K.L., Haney, M., Stone, J., Thurber, C., and Ronchin, E., 2012. Nonlinear](#)
1253 [estimation of geometric parameters in FEMs of volcano deformation: Integrating tomography models](#)
1254 [and geodetic data for Okmok volcano, Alaska. *Journal of Geophysical Research: Solid Earth*,](#)
1255 [117\(B2\).](#)
- 1256
- 1257 [Medina-Martínez, F., Espíndola, J.M., De la Fuente, M., Mena, M., 1996. A gravity model of the](#)
1258 [Colima, México region. *Geofis. Int.* 35\(4\), 409–414.](#)
- 1259 [Michaeli, W., 1991. *Extrusionswerkzeuge für Kunststoffe und Kautschuk: Bauarten, Gestaltung und*](#)
1260 [Berechnungsmöglichkeiten. Hanser Verlag.](#)

Codice campo modificato

1261
1262 [Moeck, I., Schandelmeier, H. and Holl, H.G., 2009. The stress regime in a Rotliegend reservoir of](#)
1263 [the Northeast German Basin. Int. J. Earth. Sci. 98, 1643-1654.](#)

1264 [Mutter, J.C., Carbotte, S.M., Su, W.S., Xu, L.Q., Buhl, P., Detrick, R.S., Kent, G.M., Orcutt, J.A.,](#)
1265 [Harding, A.J., 1995. Seismic images of active magma systems beneath the East Pacific Rise between](#)
1266 [17-degrees-05's and 17-degrees-35's. Science 268, 391-395.](#)

1267 [Newman, A. V., Dixon, T. H., Ofoegbu, G. I., and Dixon, J. E., 2001. Geodetic and seismic constraints](#)
1268 [on recent activity at Long Valley Caldera, California: evidence for viscoelastic rheology. Journal of](#)
1269 [Volcanology and Geothermal Research, 105\(3\), 183-206.](#)

1270
1271 [Norini, G., Agliardi, F., Crosta, G., Groppelli, G., and Zuluaga, M.C., 2019. Structure of the Colima](#)
1272 [Volcanic Complex: Origin and Behaviour of Active Fault Systems in the Edifice. In Volcán de Colima](#)
1273 [\(pp. 27-54\). Springer, Berlin, Heidelberg.](#)

1274
1275 [Norini G, Capra L, Groppelli G, Agliardi F, Pola A, Cortes A., 2010. Structural architecture of the](#)
1276 [Colima Volcanic Complex. J Geophys Res 115, B12209.](#)

1277
1278 [Núñez-Cornú F, Nava FA, De la Cruz-Reyna S, Jiménez Z, Valencia C, García-Arthur R., 1994.](#)
1279 [Seismic activity related to the 1991 eruption of Colima Volcano, Mexico. Bull Volcanol 56: 228-237.](#)

1280
1281 [Parfitt, E. A., and L. Wilson, 2008. "The role of volatiles." Fundamentals of Physical Volcanology,](#)
1282 [64-76.](#)

1283
1284 [Pinel, V., and Jaupart, C., 2004. Magma storage and horizontal dyke injection beneath a volcanic](#)
1285 [edifice. Earth and Planetary Science Letters, 221\(1-4\), 245-262.](#)

1286
1287 [Pinel, V., Carrara, A., Maccaferri, F., Rivalta, E., and Corbi, F., 2017. A two-step model for dynamical](#)
1288 [dike propagation in two dimensions: Application to the July 2001 Etna eruption. Journal of](#)
1289 [Geophysical Research: Solid Earth, 122\(2\), 1107-1125.](#)

1290
1291 [Pritchard, M. E., and Simons, M., 2004. An InSAR-based survey of volcanic deformation in the central](#)
1292 [Andes. Geochemistry, Geophysics, Geosystems, 5\(2\).](#)

1293
1294 [Rao S.S., 1989. The Finite Element Method in Engineering second edition. PERGAMON PRESS 1989](#)
1295 [ISBN 0-08-033419-9.](#)

1296
1297 [Rao, S.S., 2013. The Finite Element Method in Engineering: Pergamon International Library of](#)
1298 [Science, Technology, Engineering and Social Studies. Elsevier.](#)

1299
1300 [Reubi, O., Blundy, J., and Varley, N.R., 2013. Volatiles contents, degassing and crystallisation of](#)
1301 [intermediate magmas at Volcan de Colima, Mexico, inferred from melt inclusions. Contributions to](#)
1302 [Mineralogy and Petrology, 165\(6\), 1087-1106.](#)

1303
1304 [Reubi, O., Blundy, J., and Pickles, J., 2019. Petrological monitoring of Volcán de Colima magmatic](#)
1305 [system: the 1998 to 2011 activity. In Volcán de Colima \(pp. 219-240\). Springer, Berlin, Heidelberg.](#)
1306 [Rivalta et al., 2019. Stress inversions to forecast magma pathways and eruptive vent location Sci. Adv.](#)
[2019; 5:eau9784.](#)

1307 [Rivalta, E., Corbi, F., Passarelli, L., Acocella, V., Davis, T., and Di Vito, M.A., 2019. Stress inversions to forecast magma pathways and eruptive vent location. *Science advances*, 5\(7\), eaau9784.](#)

1308

1309

1310 [Robin, C., Mossand, P., Camus, G., Cantagrel, J. M., Gourgaud, A., and Vincent, P.M., 1987. Eruptive history of the Colima volcanic complex \(Mexico\). *Journal of Volcanology and Geothermal Research*, 31\(1-2\), 99-113.](#)

1311

1312

1313

1314 [Ronchin, E., Masterlark, T., Molist, J. M., Saunders, S., and Tao, W., 2013. Solid modeling techniques to build 3D finite element models of volcanic systems: an example from the Rabaul Caldera system, Papua New Guinea. *Computers & Geosciences*, 52, 325-333.](#)

1315

1316

1317

1318 [Ronchin, E., Geyer, A., and Martí, J., 2015. Evaluating topographic effects on ground deformation: insights from finite element modeling. *Surveys in Geophysics*, 36\(4\), 513-548.](#)

1319

1320

1321 [Rosas-Elguera, J., Ferrari, L., Garduño-Monroy, V.H., Urrutia-Fucugauchi, J., 1996: Continental boundaries of the Jalisco block and their influence in the Pliocene-Quaternary kinematics of western Mexico. *Geology* 24, 921-924.](#)

1322

1323

1324 [Rosas-Elguera J, Ferrari L, Martinez ML, Urrutia-Fucugauchi J., 1997. Stratigraphy and tectonics of the Guadalajara region and triple- junction area, western Mexico. *Int Geol Rev* 39:125-140. doi:10.1080/00206819709465263.](#)

1325

1326

1327 [Rosas-Elguera, J., Alva-Valdivia, L. M., Goguitchaichvili, A., Urrutia-Fucugauchi, J., Ortega-Rivera, M. A., Prieto, J.C.S., and Lee, J.K., 2003. Counterclockwise rotation of the Michoacan Block: implications for the tectonics of western Mexico. *International Geology Review*, 45\(9\), 814-826.](#)

1328

1329

1330

1331 [Roverato, M., Capra, L., Sulpizio, R., Norini, G., 2011. Stratigraphic reconstruction of two debris avalanche deposits at Colima Volcano \(Mexico\): insights into pre-failure conditions and climate influence. *Journal of Volcanology and Geothermal Research*, 207\(1-2\), 33-46, 2011](#)

1332

1333

1334 [Roverato, M., and Capra, L., 2013. Características microtexturales como indicadores del transporte y emplazamiento de dos depósitos de avalancha de escombros del Volcán de Colima \(México\). *Revista mexicana de ciencias geológicas*, 30\(3\), 512-525.](#)

1335

1336

1337

1338 [Salzer J.T., Nikkhoo M., Walter T., Sudhaus H., Reyes-Dávila G., Bretòn-Gonzalez M., Aràmbula R., 2014. Satellite radar data reveal short-term pre-explosive displacements and a complex conduit system at Volcan de Colima, Mexico. *Front Earth Sci* 2:12.](#)

1339

1340

1341

1342 [Saada, A.S., 2009. Elasticity: Theory and Applications. Krieger, Malabar, Florida.](#)

1343

1344

1345 [Saucedo R, Macías J., Gavilanes JC, Arce JL, Komorowski JC, Gardner JE, Valdez-Moreno G., 2010. Eyewitness, stratigraphy, chemistry, and eruptive dynamics of the 1913 Plinian eruption of Volcán de Colima, México. *J Volcanol Geotherm Res* 191:149-166.](#)

1346

1347

1348

1349 [Saucedo R, Macías JL, Gavilanes JC, Arce JL, Komorowski JC, Gardner JE, and Valdez-Moreno G., 2011. Corrigendum to Eyewitness, stratigraphy, chemistry, and eruptive dynamics of the 1913 plinian eruption of Volcan de Colima, Mexico. *J Volcanol Geotherm Res* 191:149-166.](#)

1350

1351

1352

1353 [Schwarz, H.R., 1991. Methode der finiten Elemente neubearbeitete Auflage, B.G. Teubner Stuttgart](#)
1354 [ISBN 3-519-22349-X.](#)

1355 [Selvans, M. M., Stock, J. M., DeMets, C., Sanchez, O., and Marquez-Azua, B., 2011. Constraints on](#)
1356 [Jalisco Block motion and tectonics of the Guadalajara triple junction from 1998–2001 Campaign GPS](#)
1357 [Data. Pure and applied geophysics, 168\(8-9\), 1435-1447.](#)

1358

1359 [Serpa, L., Smith, S., Katz, C., Skidmore, C., Sloan, R., Pavlis, T., 1992. A geophysical investigation](#)
1360 [of the southern Jalisco block in the state of Colima, Mexico. Geofisica Internacional 31, 247–252.](#)

1361 [Simms MA., and Graven G., 2004. Thermal convection in faulted extensional sedimentary basins:](#)
1362 [theoretical results from finite-element modelling. Geofluids \(2004\), 4, 109-130.](#)

1363

1364 [Singh, S. C., Crawford, W. C., Carton, H., Seher, T., Combier, V., Cannat, M., and Miranda, J. M.,](#)
1365 [2006. Discovery of a magma chamber and faults beneath a Mid-Atlantic Ridge hydrothermal field.](#)
1366 [Nature, 442\(7106\), 1029.](#)

1367

1368 [Sinton, J.M., and Detrick, R.S., 1992. Mid-ocean ridge magma chambers. Journal of Geophysical](#)
1369 [Research: Solid Earth, 97\(B1\), 197-216.](#)

1370

1371 [Stock JM and Lee J., 1994. Do microplates in subduction zones leave a geological record? Tectonics](#)
1372 [13:1472–1487.](#)

1373 [Stoopes, G. R., and Sheridan, M.F., 1992. Giant debris avalanches from the Colima Volcanic Complex,](#)
1374 [Mexico: Implications for long-runout landslides \(> 100 km\) and hazard assessment. Geology, 20\(4\),](#)
1375 [299-302.](#)

1376

1377 [Spica, Z., Cruz-Atienza, V.M., Reyes-Alfaro, G., Legrand, D., and Iglesias, A., 2014. Crustal imaging](#)
1378 [of western Michoacán and the Jalisco Block, Mexico, from ambient seismic noise. Journal of](#)
1379 [Volcanology and Geothermal Research, 289, 193-201.](#)

1380

1381 [Spica Z, Perton M, Legrand D., 2017. Anatomy of the Colima volcano magmatic system,](#)
1382 [Mexico, Earth Planet Sci Lett 459: 1-13.](#)

1383

1384 [Suárez, G., Garcia-Acosta, V., Gaulon, R., 1994. Active crustal deformation in the Jalisco block,](#)
1385 [Mexico: evidence for a great historical earthquake in the 16th century. Tectonophysics 234, 117–12.](#)

1386 [Sulpizio, R., Lucchi, F., Forni, F., Massaro, S., and Tranne, C., 2016. Unravelling the effusive-](#)
1387 [explosive transitions and the construction of a volcanic cone from geological data: The example of](#)
1388 [Monte dei Porri, Salina Island \(Italy\). Journal of Volcanology and Geothermal Research, 327, 1-22.](#)

1389

1390 [Sulpizio, R., and Massaro, S., 2017. Influence of stress field changes on eruption initiation and](#)
1391 [dynamics: a review. Frontiers in Earth Science, 5, 18.](#)

1392

1393 [Tibaldi, A., 2015. Structure of volcano plumbing systems: A review of multi-parametric effects.](#)
1394 [Journal of Volcanology and Geothermal Research 298 \(2015\) 85–135.](#)

1395 [Touloukian, Y.S., Judd, W.R., Roy, R.F., 1989. Physical Properties of Rocks and Minerals, vol. 548.](#)
1396 [Hemisphere, New York.](#)

1397 [Turcotte, D. L. and Schubert, G., 2002. Geodynamics, 2nd edition, Cambridge University Press.](#)

1398 [Zehner B, Jana H, Börner J.H., Görz I., Spitzer K., 2015. Workflows for generating tetrahedral meshes](#)

1399 [for finite element simulations on complex geological structures. Computers and Geosciences, 79, 105-](#)
1400 [117.](#)

1401 [Zhao, S., Muller, R. D., Takahashi, Y. and Kaneda, Y., 2004. 3-D finite-element modelling of](#)
1402 [deformation and stress associated with faulting: effect of inhomogeneous crustal structures, Geophys.](#)
1403 [J. Int., 157, 629– 644.](#)

1404 [Zhong, X. Marcin, Dabrowski, Bjørn Jamtveit, 2019. Analytical solution for the stress field in elastic](#)
1405 [half space with a spherical pressurized cavity or inclusion containing eigenstrain. Geophysical](#)
1406 [Journal International \(submitted\).](#)

1407 [Zobin, V.M., Luhr, J.F., Taran, Y.A., Bretón, M., Cortés,A., De la Cruz-Reyna, S., Domínguez, T.,](#)
1408 [Galindo, I., Gavilanes, J.C., Muñoz, J.J., Navarro, C., Ramírez, J. J., Reyes, G.A., Ursúa, M., Velasco,](#)
1409 [J., Alatorre, E., Santiago, H., 2002. Overview of the 1997–2000 activity of Volcán de Colima, Mexico.](#)
1410 [J. Volcanol. Geotherm.Res. 117, 1–19.](#)

1411 [Watanabe, T., Masuyama, T., Nagaoka, K., Tahara, T., 2002. Analog experiments on magma-filled](#)
1412 [cracks: competition between external stresses and internal pressure. Earth Planets Space 54, 1247–](#)
1413 [1261.](#)

1414 [Wang, R., Martin, F.L. and Roth, F., 2003. Computation of deformation induced by earthquakes in a](#)
1415 [multi-layered elastic crust-FORTRAN programs EDGRN/EDCMP, Comput. Geosci., 29, 195–207.](#)
1416
1417

1418 [Eyewitness, stratigraphy, chemistry, and eruptive dynamics of the 1913 plinian eruption of Volcan de](#)
1419 [Colima, Mexico. J Volcanol Geotherm Res 191:149–166.](#)

1420
1421 [Schwarz, H.R., 1991. Methode der finiten Elemente neubearbeitete Auflage, B.G. Teubner Stuttgart](#)
1422 [ISBN 3-519-22349-X.](#)

1423 [Selvans, M. M., Stock, J. M., DeMets, C., Sanchez, O., and Marquez-Azua, B., 2011. Constraints on](#)
1424 [Jalisco Block motion and tectonics of the Guadalajara triple junction from 1998–2001 Campaign GPS](#)
1425 [Data. Pure and applied geophysics, 168\(8-9\), 1435-1447.](#)

1426
1427 [Serpa, L., Smith, S., Katz, C., Skidmore, C., Sloan, R., Pavlis, T., 1992. A geophysical investigation](#)
1428 [of the southern Jalisco block in the state of Colima, Mexico. Geofisica Internacional 31, 247–252.](#)

1429 [Simms MA., and Graven G., 2004. Thermal convection in faulted extensional sedimentary basins:](#)
1430 [theoretical results from finite-element modelling. Geofluids \(2004\), 4, 109-130.](#)

1431
1432 [Singh, S. C., Crawford, W. C., Carton, H., Seher, T., Combier, V., Cannat, M., and Miranda, J. M.,](#)
1433 [2006. Discovery of a magma chamber and faults beneath a Mid-Atlantic Ridge hydrothermal field,](#)
1434 [Nature, 442\(7106\), 1029.](#)

1435
1436 [Sinton, J.M., and Detrick, R.S., 1992. Mid-ocean ridge magma chambers. Journal of Geophysical](#)
1437 [Research: Solid Earth, 97\(B1\), 197-216.](#)

1438
1439 [Stock JM and Lee J., 1994. Do microplates in subduction zones leave a geological record? Tectonics](#)
1440 [13:1472–1487.](#)

1441 [Stoopes, G. R., and Sheridan, M.F., 1992. Giant debris avalanches from the Colima Volcanic Complex,](#)
1442 [Mexico: Implications for long-runout landslides \(> 100 km\) and hazard assessment. *Geology*, 20\(4\),](#)
1443 [299-302.](#)

1444

1445 [Spica, Z., Cruz-Atienza, V.M., Reyes-Alfaro, G., Legrand, D., and Iglesias, A., 2014. Crustal imaging](#)
1446 [of western Michoacán and the Jalisco Block, Mexico, from ambient seismic noise. *Journal of*](#)
1447 [Volcanology and Geothermal Research](#), 289, 193-201.

1448

1449 [Spica Z, Pertou M, Legrand D., 2017. Anatomy of the Colima volcano magmatic system,](#)
1450 [Mexico, *Earth Planet Sci Lett* 459: 1-13.](#)

1451

1452 [Suárez, G., Garcia-Acosta, V., Gaulon, R., 1994. Active crustal deformation in the Jalisco block,](#)
1453 [Mexico: evidence for a great historical earthquake in the 16th century. *Tectonophysics* 234, 117–12.](#)

1454

1455 [Sulpizio, R., Lucchi, F., Forni, F., Massaro, S., and Tranne, C., 2016. Unravelling the effusive-](#)
1456 [explosive transitions and the construction of a volcanic cone from geological data: The example of](#)
1457 [Monte dei Porri, Salina Island \(Italy\). *Journal of Volcanology and Geothermal Research*, 327, 1-22.](#)

1458

1459 [Sulpizio, R., and Massaro, S., 2017. Influence of stress field changes on eruption initiation and](#)
1460 [dynamics: a review. *Frontiers in Earth Science*, 5, 18.](#)

1461

1462 [Tibaldi, A., 2015. Structure of volcano plumbing systems: A review of multi-parametric effects.](#)
1463 [Journal of Volcanology and Geothermal Research 298 \(2015\) 85–135.](#)

1464

1465 [Touloukian, Y.S., Judd, W.R., Roy, R.F., 1989. Physical Properties of Rocks and Minerals, vol. 548.](#)
1466 [Hemisphere, New York.](#)

1467

1468 [Turcotte, D. L. and Schubert, G., 2002. Geodynamics, 2nd edition, Cambridge University Press.](#)

1469

1470 [Zehner B, Jana H, Börner J.H., Görz I., Spitzer K., 2015. Workflows for generating tetrahedral meshes](#)
1471 [for finite element simulations on complex geological structures. *Computers and Geosciences*, 79, 105-](#)
1472 [117.](#)

1473

1474 [Zhao, S., Muller, R. D., Takahashi, Y. and Kaneda, Y., 2004. 3-D finite-element modelling of](#)
1475 [deformation and stress associated with faulting: effect of inhomogeneous crustal structures. *Geophys.*](#)
1476 [J. Int., 157, 629– 644.](#)

1477

1478 [Zhong, X., Marcin, Dabrowski, Bjørn Jamtveit, 2019. Analytical solution for the stress field in elastic](#)
1479 [half space with a spherical pressurized cavity or inclusion containing eigenstrain. *Geophysical*](#)
1480 [Journal International](#) · (submitted).

1481

1482 [Zobin, V.M., Luhr, J.F., Taran, Y.A., Bretón, M., Cortés, A., De la Cruz-Reyna, S., Domínguez, T.,](#)
1483 [Galindo, I., Gavilanes, J.C., Muñoz, J.J., Navarro, C., Ramírez, J. J., Reyes, G.A., Ursúa, M., Velasco,](#)
1484 [J., Alatorre, E., Santiago, H., 2002. Overview of the 1997–2000 activity of Volcán de Colima, Mexico.](#)
1485 [J. Volcanol. Geotherm.Res. 117, 1–19.](#)

1486
1487
1488
1489
1490